Journal of Structural Geology 169 (2023) 104828

Contents lists available at ScienceDirect

Journal of Structural Geology

journal homepage: www.elsevier.com/locate/jsg

Architecture of active extensional faults in carbonates: Campo Felice and Monte D'Ocre faults, Italian Apennines

Luca Del Rio [a,*], Marco Moro [b], Simone Masoch [a], Fawzi Doumaz [b], Michele Saroli [d,b], Andrea Cavallo [c], Giulio Di Toro [a,b]

[a] Dipartimento di Geoscienze, Università degli Studi di Padova, Via G. Gradenigo 6, 35131, Padua, Italy
[b] Istituto Nazionale di Geofisica e Vulcanologia (INGV), Via di Vigna Murata 605, 00143, Rome, Italy
[c] Laboratorio tecnologico multidisciplinare CERTEMA, Grosseto, Italy
[d] DICeM-Dip. di Ingegneria Civile e Meccanica, Università di Cassino e del Lazio Meridionale, Via G. Di Biasio 43, 03043, Cassino, Italy

ARTICLE INFO

Keywords:
Normal faults
Deep-seated gravitational slope deformations
Carbonates
Damage zones
Slip zones
Apennines

ABSTRACT

To understand better the development of deformation in carbonate-hosted normal faults, we compared the structural architecture of the Campo Felice and Monte D'Ocre active faults (Italian central Apennines). The two geometrically linked structures displace the same carbonate sequences, but with different Quaternary slip rates and geological throws. Moreover, several geomorphological features typical of deep-seated landslides were identified across the Mt. D'Ocre range. The Campo Felice fault segment and the Cama fault segment (Monte D'Ocre range) consist of 0.4–15 m thick and almost absent fault cores and of >400 m and <40 m thick damage zones, respectively. The associated slip zones have different fabrics (i.e., cataclasite *vs.* crush fault breccia for Campo Felice and Cama Fault, respectively). The different fault zone architecture and associated landscapes would suggest different behaviors of the two faults although similar deformation mechanisms (i.e., cataclasis and pressure-solution) are active in both the two scarps. The Mt. D'Ocre faults would not be segments of the Ovindoli-L'Aquila Fault System and currently accommodate the lateral spreading of the Mt. D'Ocre ridge. Therefore, the seismic hazard associated with the fault system might be reduced. This work shows how macro-to micro-structural analyses provide further information to improve the structural characterization of seismogenic sources.

1. Introduction

Analysis of natural exposures of fault zones is the best tool to image fault internal structure and to interpret the physical processes associated with fault growth and possibly the ancient seismic activity (Kim et al., 2004; Wibberley et al., 2008; Rowe and Griffith, 2015; Ferraro et al., 2019, 2020; La Bruna et al., 2018; Masoch et al., 2021, 2022). Instead, microstructural analysis of slip zones allows geologists to investigate the deformation mechanisms active during fault zone lifetime (e.g., Sibson, 1986; Di Toro and Pennacchioni, 2005; Smith et al., 2011; Tesei et al., 2013; Clemenzi et al., 2015; Leah et al., 2018; Masoch et al., 2019; Ferraro et al., 2019, 2020; Fondriest et al., 2020).

The Italian central Apennines are one of the most seismically active regions in Europe, with an average recurrence of one moderate-to large-in-magnitude ($M_w \geq 5.5$) earthquake per decade (Rovida et al., 2020). Most of the Apennines active normal faults strike NW-SE and are often disposed in an en-échelon array forming up to 30-km-long fault systems (Boncio et al., 2004, Fig. 1a). Individual fault segments interact with each other and may rupture either independently or together during a seismic sequence. For example, during the Amatrice-Norcia 2016–2017 seismic sequence in the northern Apennines, the M_w 6.5 Norcia October 30, 2016 earthquake, that ruptured the whole Mt. Vettore-Mt. Bove fault system (~28-km-long and composed of three fault segments), was preceded by the M_w 6.0 Amatrice August 24, 2016 earthquake in the southern segment and by the M_w 5.9 Visso October 26, 2016 earthquake in the northern segment (Chiaraluce et al., 2017; Villani et al., 2018). Few tens of kilometers to the South, the most recent earthquake that hit the central Apennines was the M_w 6.1 L'Aquila April 6, 2009 earthquake, whereas the largest one instrumentally recorded was the M_w 7.0 Avezzano, 1915 earthquake (EWG, 2010, Fig. 1a).

In the area comprised between the Ovindoli and L'Aquila towns, three major fault segments (namely, from north to south: Mt. D'Ocre

* Corresponding author.
E-mail address: Luca.delrio@studenti.unipd.it (L. Del Rio).

https://doi.org/10.1016/j.jsg.2023.104828
Received 20 July 2022; Received in revised form 13 February 2023; Accepted 16 February 2023
Available online 23 February 2023

faults, Campo Felice fault and Ovindoli-Pezza fault; Bosi et al., 1993; Pantosti et al., 1996; Salvi et al., 2003), arranged in a right-stepping en-échelon array, form the 27-km-long Ovindoli-L'Aquila Fault System (OAFS; Fig. 1a; also referred as Celano-L'Aquila Fault System in Salvi and Nardi, 1995, and Cerasitto-Campo Felice-Ovindoli-Pezza Fault System in Galli et al., 2008). Thanks to the good correlation among the ages of the Late Pleistocene-Holocene paleo-earthquakes with those recognized along the Ovindoli-Pezza fault (Pantosti et al., 1996), the Mt.

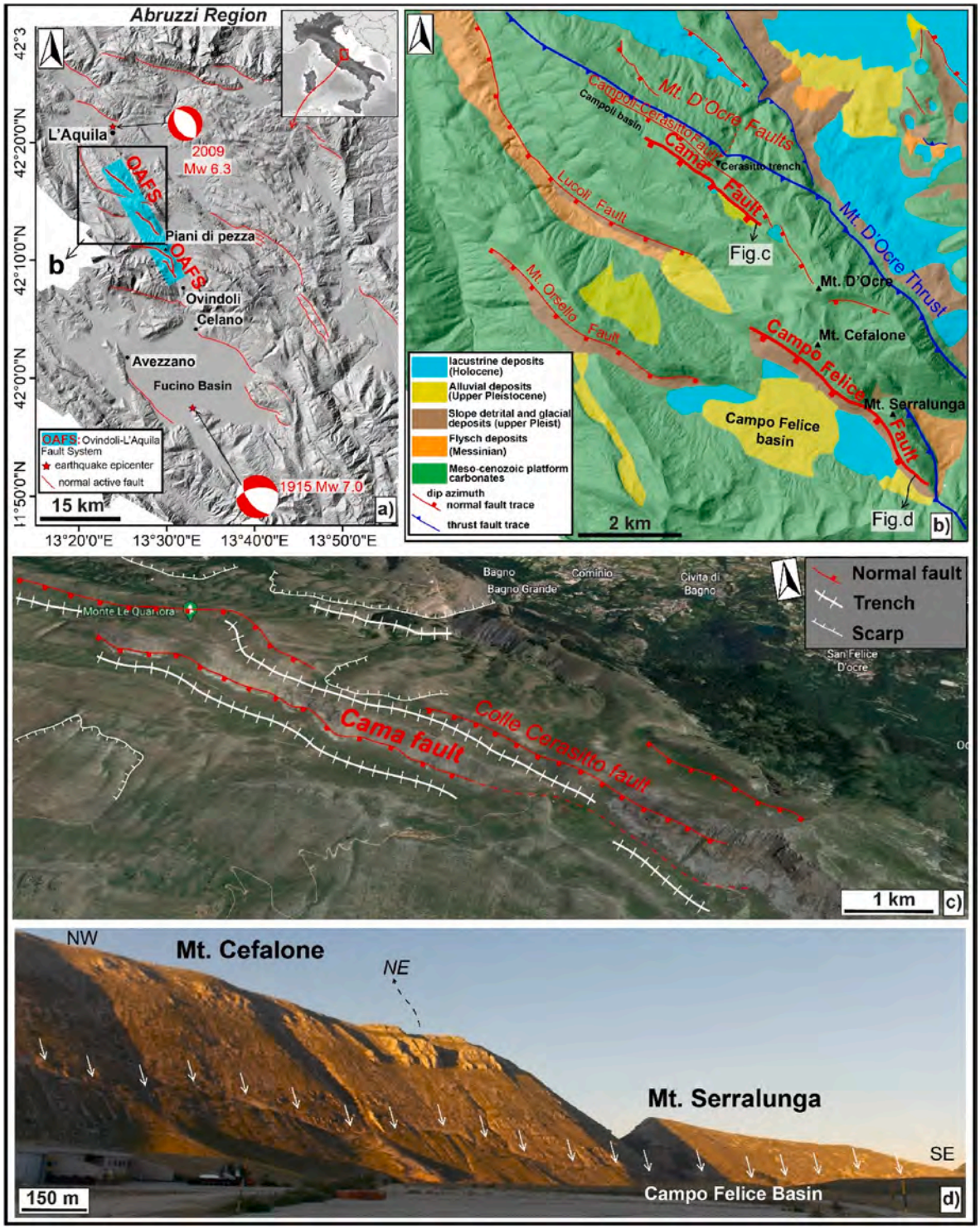

Fig. 1. Geological setting of the Campo Felice and Mt. D'Ocre Faults. a) Seismotectonic map of the study area (Abruzzi Region) with indicated the main Quaternary active faults (red lines). Thicker red lines indicate the Ovindoli-L'Aquila Fault System (OAFS). Focal mechanisms indicate the mainshocks of the largest (i.e., Avezzano $M_w = 7.0$, 1915) and most recent (i.e., L'Aquila $M_w = 6.1$, 2009) earthquakes striking the region from 1900. b) Simplified geological map of the area with the Campo Felice and Cama faults (thicker red lines), investigated in this work. c) Panoramic view of the Mt. D'Ocre range, with associated geomorphological features typical of DGSDs, such as scarps and gravitative trenches. d) Surface expression of the Campo Felice fault scarp, affecting the SW slopes of Cefalone and Serralunga Mts. and bordering the homonym intermontane basin. (For interpretation of the references to color in this figure legend, the reader is referred to the Web version of this article.)

D'Ocre faults were interpreted as the northern segment of the OAFS (Salvi et al., 2003). Thus, the Campo Felice and Ovindoli-Pezza faults represent the central and southern segments of the OAFS, respectively (Salvi et al., 2003).

In detail, the Campo Felice and Mt. D'Ocre faults displace the same Cretaceous carbonate sequence with similar kinematics, but have (i) different throw rates (1.1 mm/yr vs. 0.2 mm/yr, respectively, estimated in the last 18.000 years; Galadini and Galli, 2000; Salvi et al., 2003) and (ii) border valleys with different shapes and dimensions (i.e., the 20-km^2-wide Campo Felice intermontane basin vs. the <400-m^2-wide valleys of the Mt. D'Ocre range; Figs. 1 and 2). Moreover, several geomorphological features typical of Deep-seated Gravitational Slope Deformations (DGSDs), such as gravitative trenches, double-crested lines, bulging, up-hill and down-hill facing scarps (Hutchinson, 1988) are recognizable across the Mt. D'Ocre range (Salvi and Nardi, 1995; Salvi et al., 2003, Fig. 1c). In particular, Albano et al. (2015) documented a gravitational subsidence of tens of millimeters of the Mt. D'Ocre ridge toward the L'Aquila Plain in the months following the L'Aquila mainshock (see Fig. 7 in Albano et al., 2015).

Specifically, DGSDs are deep gravitational landslides involving hundreds of meters thick rock volumes moving from the ridge-top to the valley floor (Jahn, 1964; Zischinsky, 1966; 1969; Varnes, 1978; Hutchinson, 1988; Dramis and Sorriso-Valvo, 1994; Jaboyedoff et al., 2013; Panek and Klimeš, 2016; Discenza and Esposito, 2021). DGSDs differs from other types of landslides by both the absence of continuous and well-defined external boundaries (Agliardi et al., 2001, 2012; Crosta et al., 2013) and the lack of a continuous sliding surface or basal shear zone (Dramis and Sorriso-valvo, 1994; Discenza and Esposito, 2021), that is commonly buried by the rock-mass and thus almost impossible to recognize, especially in lateral spreading DGSDs. The latter usually form when a rigid and joined rock-mass gently overlaps a more ductile and highly deformable bedrock (Varnes, 1978; Hutchinson, 1988; Agliardi et al., 2012; Bozzano et al., 2013; Di Maggio et al., 2014).

As a result, the Campo Felice and Mt. D'Ocre extensional faults represent a great opportunity to compare the fault zone associated with two geometrically linked structures displacing the same carbonate rocks, but with different (i) slip rates, (ii) cumulated displacement and (iii) associated morphological features. The internal structure of brittle fault zones commonly includes two main structural units: fault core and damage zone (Caine et al., 1996; Faulkner et al., 2003; Sibson, 2003). The fault core is the high-strain domain usually composed of low-permeability fault rocks (fault gouges, cataclasites and fault breccias) where most of the displacement is accommodated (Ferraro et al., 2018). Instead, the damage zone consists of variably fractured rock volumes where brittle deformation is accommodated by secondary faults and fractures (Chester and Logan, 1986; Agosta and Aydin, 2006; Faulkner et al., 2010; Billi et al., 2003; Choi et al., 2016; Ferraro et al., 2018). In general, the intensity of deformation decreases broadly exponentially from the fault core of the master fault towards the damage zone (Chester and Logan, 1986; Chester et al., 1993; Caine et al., 1996; Faulkner et al., 2003; Wibberley et al., 2008; Mitchell and Faulkner, 2009; Savage and Brodsky, 2011; Demurtas et al., 2016; Gomila et al.,

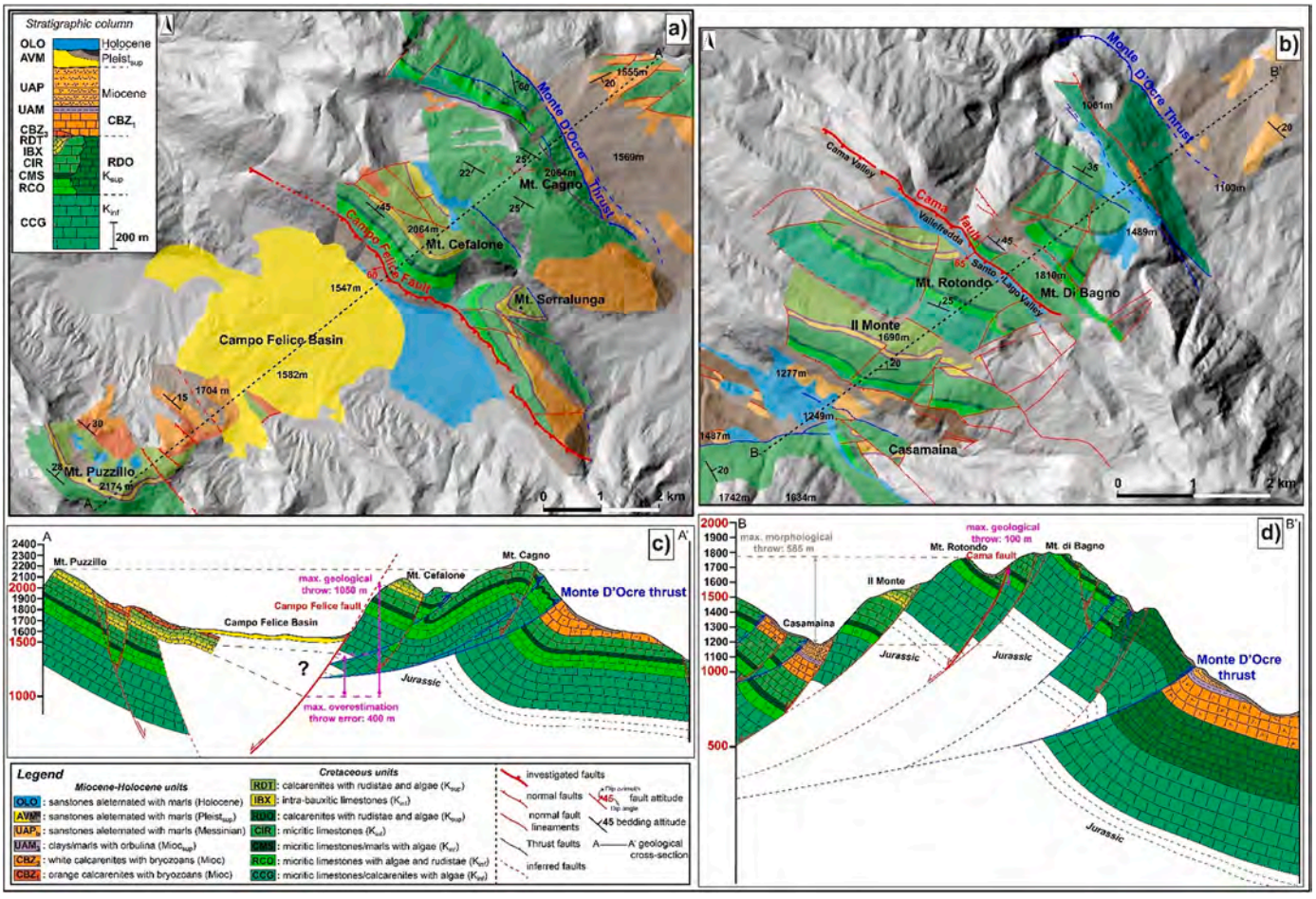

Fig. 2. Simplified geological maps of the areas affected by the Campo Felice (a) and Mt. D'Ocre (b) faults, including stratigraphic column and trace of the cross-sections. Data are compiled from the 1:50.000 scale "Foglio 359 L'Aquila" (ISPRA). c) Cross-section A-A′, showing the Campo Felice fault cutting Cretaceous platform carbonates with a maximum estimated geological throw of ~1050 m (with a possible overestimate of ~400 m). d) Cross-section B–B′, cutting the entire Mt. D'Ocre range, at the hanging wall of the Mt. D'Ocre thrust. The Cama fault displaces Cretaceous carbonates with ~100 m of geological throw.

2016; Fondriest et al., 2020; Ostermeijer et al., 2020).

In this work, we map and compare the distribution of fractures affecting the footwall blocks of the Campo Felice fault and the south-western branch of the Mt. D'Ocre faults (i.e., the Cama fault segment; Fig. 1) and analyze the microstructures of the slip zones associated with the major slip surfaces. The analysis of the deformation processes at macro-to micro-metric scale (from km to nm) associated with the Campo Felice and Cama fault scarps may contribute to shed more light on 1) the formation and current mechanical behavior of the two faults in the tectonic context of the central Apennines and their relation and, 2) the deformation mechanisms active in the slip zones of carbonate-hosted normal faults as a function of fault displacement. These kinds of studies may find more general application to other areas worldwide characterized by moderate to strong seismicity in carbonate rocks (Caputo et al., 2006, 2010; Verhaert et al., 2009; Rotevatn and Bastesen, 2012). Finally, the possible interpretation of certain sharp scarps as surface expression of seismic or aseismic faulting (i.e., normal faults vs. DGSDs; Del Rio et al., 2021) may have strong implications on the characterization of the potential seismogenic source of the area and, thus, to determine the maximum moment magnitude of the earthquake that the fault system can produce (Wells and Coppersmith, 1994; Boncio et al., 2004; Galadini et al., 2012; Falcucci et al., 2016).

2. Geological setting

2.1. Tectonics of the Apennines

The Italian Apennine fold-and-thrust belt started to develop since Miocene, due to the NE-verging collision between the Adriatic and European Plates (Elter et al., 1975; Patacca et al., 1992; Carminati et al., 2012). The Apennine orogenesis was characterized by a general eastward migration of the chain thrust front and consequent formation of piggy-back basins associated with the main thrusts (Cosentino et al., 2010). In the central Apennines, during this compressional phase, shallow-water and pelagic Mesozoic-Cenozoic limestones were juxtaposed to syn-orogenic foredeep deposits by NE-verging thrusts (Cosentino et al., 2010). Since Upper Messinian to present, a NE oriented crustal extension accommodated the stretching of the Apennine chain, caused by the retreat of the subduction hinge toward E-NE (Malinverno and Ryan, 1986; Carminati and Doglioni, 2012). During Quaternary, a strong increase in regional uplift (i.e., more than 1000 m; D'Agostino et al., 2001) lead to the formation of large intermontane basins filled with continental deposits, bordered by active normal faults (Demangeot, 1965; Dramis, 1992; Galadini and Galli, 2003). The combination of extensional faulting (Quaternary extension rate of 2–3 mm/yr; Hunstad et al., 2003) and regional uplift is the main cause of the development of DGSDs in the central Apennines (Galadini, 2006).

The current extensional tectonic phase is accommodated by active normal faults cutting and locally exploiting the inherited Miocene-Early Pleistocene thrusts and the earlier Mesozoic normal faults (Elter et al., 1975; Vezzani et al., 2010; Leah et al., 2018; Lucca et al., 2019; Fondriest et al., 2020). Most of the active faults in central Apennines strike NW-SE (i.e., "Apennine trend") and are commonly organized in fault systems with associated intermontane basins (e.g., Campo Felice and Middle Aterno Basins; Bosi et al., 1993; Cavinato et al., 2002). Smaller NE-SW oriented normal faults (i.e., "anti-Apennine trend") are also spread in the area.

2.2. Campo Felice and Mt. D'Ocre faults

In the area affected by the Campo Felice and Mt. D'Ocre Faults, Cretaceous and Miocene shallow-water carbonates belonging to the Latio-Abruzzi succession crop out. The carbonate sequence is locally capped by Upper Miocene hemipelagic marls and Messinian flysch deposits (Cosentino et al., 2010; Brandano, 2017, Fig. 1b; 2a, b). The Cretaceous Units record the sedimentation in shallow-water platform environments along the passive margin of the Adriatic plate, started during Middle Liassic. These units mainly consist of micritic limestones alternated with thin levels of calcarenites or marls, with bedding thickness ranging from tens of centimetres to over 1 m (see stratigraphic column in Fig. 2a). During the Lower Albian-Early Cenomanian, this carbonate platform underwent three periods of aerial exposure and erosion of the underlying limestones, with consequent formation of karst cavities filled with bauxitic deposits (i.e., IBX fm. in Fig. 2; Mancinelli et al., 2003). Middle Miocene carbonates (i.e., "*Calcari a Briozoi e Litotamni*" Formation) consist of thin whitish calcarenites including bryozoans, lithotamnia and corals (Fig. 2a) that deposited unconformably or para-conformably above the Cretaceous limestones (i.e., "Paleogene Hiatus"; Damiani et al., 1992). Miocene hemipelagic marls record the gradual drowning of the carbonate ramp with consequent increase in clay amount at the expense of lime portion. During Messinian, siliciclastic turbidites filled the foredeep basins according to the eastern migration of the Apennine chain thrust front (Patacca and Scandone, 1989, Figs. 1b and 2a).

The Campo Felice Fault strikes NW-SE for ~6 km, cutting the south-western flanks of Mt. Serralunga, to SE, and Mt. Cefalone, to NW (Fig. 1b, d; 2a). The fault has a normal dip-slip kinematics (Wilkinson et al., 2015) and juxtaposes Cretaceous shallow-water limestones with talus and slope sediments deposited during and after the Last Glacial Maximum (i.e., ~25.000–21.000 B.P.; Dramis, 1983). The Campo Felice fault borders to SW the homonym intermontane basin (~20 km^2 wide), filled with Late Pleistocene to Holocene alluvial, lacustrine and glacial deposits (Giraudi et al., 2011, Figs. 1b and 2a). The Mt. D'Ocre thrust borders the north-eastern side of Serralunga and Cefalone Mts. juxtaposing pre-orogenic calcareous units with syn-orogenic calcareous and siliciclastic deposits (Figs. 1b and 2a, c).

The Mt. D'Ocre range is composed of three parallel and discontinuously outcropping bedrock scarps, from the Mt. D'Ocre, to SE, to the Campoli Basin, to NW, affecting the same rocks of the Campo Felice fault (Salvi et al., 2003, Fig. 1b, d; 2b). The largest scarp belongs to the Campoli-Cerasitto fault (~9.5 km long along-strike), that borders to SW the Campoli Basin in the northwestern sector (Salvi et al., 2003, Fig. 1b). Instead, the Cama fault is ~ 3-km-long and borders three small and narrow valleys (i.e., Cama, Vallefredda and Santo Lago valleys to SW), possibly produced by the gravitational spreading of the ridge-top (Salvi et al., 2003, Fig. 2b).

3. Methods

We realized two geological maps of the area affected by the Campo Felice and the Mt. D'Ocre faults (Fig. 2a and b) by editing and drawing the geological and stratigraphic information reported in the 1:50.000 scale geological map from ISPRA ("Foglio 359 L'Aquila") over a shaded relief from TINITALY (Triangular Irregular Network of Italy) 10-m-resolution digital elevation model (Tarquini et al., 2007). From the geological maps, we built two cross-sections oriented perpendicular to the strike of the Campo Felice and Mt. D'Ocre faults, respectively, to estimate the geological throw (i.e., the vertical component of displacement) and identify possible differences at regional scale associated with the two structures. The geological throw was calculated as the elevation difference between the hanging wall and footwall cutoffs of a selected Cretaceous unit (Fig. 2c and d). We assumed a constant thickness of the geological units across the two sections.

High-resolution georeferenced orthomosaics (spatial resolution of ~3 cm/pixel) of Cefalone and Serralunga Mts. and the ridge crest affected by the Cama fault were produced by stitching hundreds of either nadir-directed and fault plan-parallel photographs taken with a MAVIC 2 Pro drone and processed with Agisoft Metashape Pro software. The Stitching or Mosaicking process has been made possible thanks to photogrammetric processing, producing hence, a high-resolution DEM and 3D mesh used as base to ortho-rectify the final mosaic of the drone pictures. Original field structural surveys were conducted to map the

footwall block of the Campo Felice and Cama faults. We defined five main structural units based on field observations, such as: 1) average spacing among fractures 2) clast/matrix proportion in the fault rocks and 3) degree of preservation of primary sedimentary structures (Fig. 3). The trace of master fault scarps and of larger secondary faults (i.e., faults with lateral continuity >2 m and with a fault core associated), and the spatial distribution of the different structural units were reported in topographic maps at 1:1000 scale (spatial resolution of 0.2 m/pixel) provided by the Abruzzi Geoportal (www.geoportale.regione.abruzzo.it). These data were digitalized with ArcGIS 10.7.1 software, using the produced orthomosaics as base map, to realize detailed structural maps of the footwall blocks of the Campo Felice and Cama fault zones. The distribution of the structural units was drawn with higher degree of transparency where they were not directly observed, but inferred during the field surveys. Three structural-geological cross-sections across the analyzed fault zones were produced (Figs. 4–6).

Structural data (n = 3047) were collected along the whole along-strike path of the outcropping master fault scarps and across the footwall damage zones and located with a handheld GPS (accuracy ± 2 m). We systematically measured the attitude of different structural and stratigraphic elements (i.e., bedding, fractures, major and secondary faults, veins, stylolites). Where possible, the kinematic of the secondary faults was measured through kinematic indicators, such as S–C fabrics, grooves, slickenlines and/or calcite slickenfibers (Chester and Logan, 1986; Petit, 1987). Structural measurements were plotted and analyzed using stereonets (lower hemisphere, Schmidt equal area) created with OSX Stereonet software (Allmendinger et al., 2011; Cardozo and Allmendinger, 2013).

From 30 samples collected from the major and secondary faults, we selected 14 samples to produce syton-polished thin sections cut perpendicular to the slip surface and parallel to the kinematic indicators (where recognizable, otherwise along the fault dip direction). The thin sections were photo-scanned at high resolution (4000 dots per inch) both in plane and cross polarized Nicols and edited using specific tools of Adobe Photoshop to highlight the clast shapes, minor fractures and veins and the texture of the fine matrix surrounding the clasts.

Transmitted-light optical microscopy (OM) was used to determine microstructural features at thin section scale and to identify areas suitable for microanalytical investigations. Scanning electron microscopy (SEM) was used to acquire high-resolution backscattered electron (BSE) images coupled with both semiquantitative and quantitative energy dispersion spectroscopy (EDS) elemental analysis. SEM investigation were performed with a CamScan MX3000 (max. resolution ~50 μm in back-scatter electrons) installed at Dipartimento di Geoscienze (Università degli Studi di Padova, Padova, Italy) and with the field-emission SEM (FESEM) Merlin Zeiss (resolution of 10–100 nm in Back-Scatter electrons, BSe, and of 300 nm to 1 μm in X-rays) installed at CERTEMA laboratory (Grosseto, Italy). The images were taken with an acceleration voltage of 15 kV and a working distance of 8.5–5.3 mm.

4. Results

In this section, we describe two geological sections cross-cutting the Campo Felice and Cama fault zones, the fault architecture in the footwall blocks and the microstructures observed in the slip zones associated with the major and secondary fault surfaces. Faults traced with dashed lines in the cross-sections indicate both the faults inferred in map and the interpreted prosecution of the major faults at depth. In the case of two normal faults with opposite dip direction and crossing each other at depth, we interpret the normal fault with higher displacement as cutting the one with lower displacement.

4.1. Geological cross-sections

The cross-section A-A' (~8-km-long) is oriented SW-NE from Mt. Puzzillo to Mt. Cagno and crosses the Campo Felice basin, the Campo Felice fault, the central sector of Mt. Cefalone and the Mt. D'Ocre thrust (Fig. 2a, c). Unfortunately, though active seismic investigations were conducted by the Istituto Nazionale di Geofisica e Vulcanologia in 2019–2021, no geological and geophysical data are currently available to infer the Cretaceous-Miocene stratigraphy and possible secondary structures in the Campo Felice basin. Therefore, assuming a constant dip of ~30° of the geological Units, we estimate a maximum geological throw of ~1050 m associated with the Campo Felice fault in this sector (with a possible overestimate of ~400 m in case of sub-horizontal dip) from the elevation difference between hanging wall and footwall cutoffs of the Cenomanian Intrabauxitic limestones (IBX fm.; Fig. 2c). Because of the large displacement associated, we assumed that the Campo Felice fault cuts the Mt. D'Ocre thrust at depth. Instead, we interpret the other normal faults at the hanging wall of the Campo Felice fault to flatten at depth along the Mt. D'Ocre thrust because of their lower displacement. Here, the latter puts in contacts Lower Cretaceous shallow-water carbonates with Upper Miocene syn-orogenic limestones forming a large ramp anticline cut by small faults with tens of meters of displacement (Fig. 2c).

The cross-section B–B' (~7.25-km-long) cross-cuts the entire Mt. D'Ocre range, located at the hanging wall of Mt. D'Ocre thrust. In our geological map (Fig. 2b), we trace the Cama fault up to the south-eastern termination of the Santo Lago Valley for two reasons: (1) the stratigraphic relations among Cretaceous carbonates infer the presence of a SW-dipping normal fault with a geological throw of ~100 m (Fig. 2d); (2) the presence of a sharp fault scarp cropping out discontinuously along the western slope of Vallefredda and Santo Lago Valleys (Figs. 1c and 5). Because of the relatively low associated displacement, the Cama fault was interpreted to flatten on the Mt. D'Ocre thrust at depth, as well as the other normal faults of the Mt. D'Ocre Range (Fig. 2d). The latter juxtaposes shallow water Cretaceous carbonates with Messinian turbiditic deposits (Fig. 2b, d). According to our interpretation, the Mt. D'Ocre thrust does not flatten on turbidites, but forms a ramp to accommodate the folding of both Cretaceous and Miocene Units (Marshak et al., 2019). The maximum morphological throw associated with the faults bordering the western side of Il Monte and Rotondo Mts. is ~600 m, calculated from the elevation difference between the top of Mt. Rotondo and the lower portion of the basin hosting the Casamaina Village (Fig. 2d).

4.2. Fault zones architecture

In this section, we describe the spatial distribution and attitude of secondary faults and fractures in the footwall of the Campo Felice and Cama fault zones (~6 km and ~3 km long, respectively; Fig. 1). Though the two faults cut the same host rocks (Figs. 1 and 2), their fault architecture (i.e., core and damage zone thickness and distribution, type and intensity of fault/fracture network) may suggest different formation mechanism, evolution and deformation styles. We use the terms open fractures or fissures to indicate fractures with >1 cm of aperture between the two opposite fracture surfaces, locally filled by unconsolidated soil deposits (e.g., Figs. 3a and 7h; Fossen, 2010). Instead, extensional (or Mode-1) fractures refer to regularly spaced fractures with similar attitude, forming specific sets, with no displacement between the fracture surfaces (Engelder, 1987; Pollard and Aydin, 1988; Fossen, 2010). The five main structural units identified in the field are described from the lower to higher strained ones as follows:

Host rocks with fissures (brown in the structural maps; e.g., Figs. 3 and 6) consist of rock volumes where intact carbonate strata are affected by sub-vertical (>60°) fractures and fissures spaced >20 cm apart, with fracture surfaces very rough due to karst-related processes (Fig. 3a).

Weakly fractured rocks (light blue in the structural maps; e.g., Figs. 3–6) consist of poorly fractured rock volumes, where bedding is clearly recognizable and not affected by fractures, which are usually spaced >10 cm apart and oriented at high angles (i.e., 60°–90°) with respect to the bedding surfaces, as a result forming lozenge-like

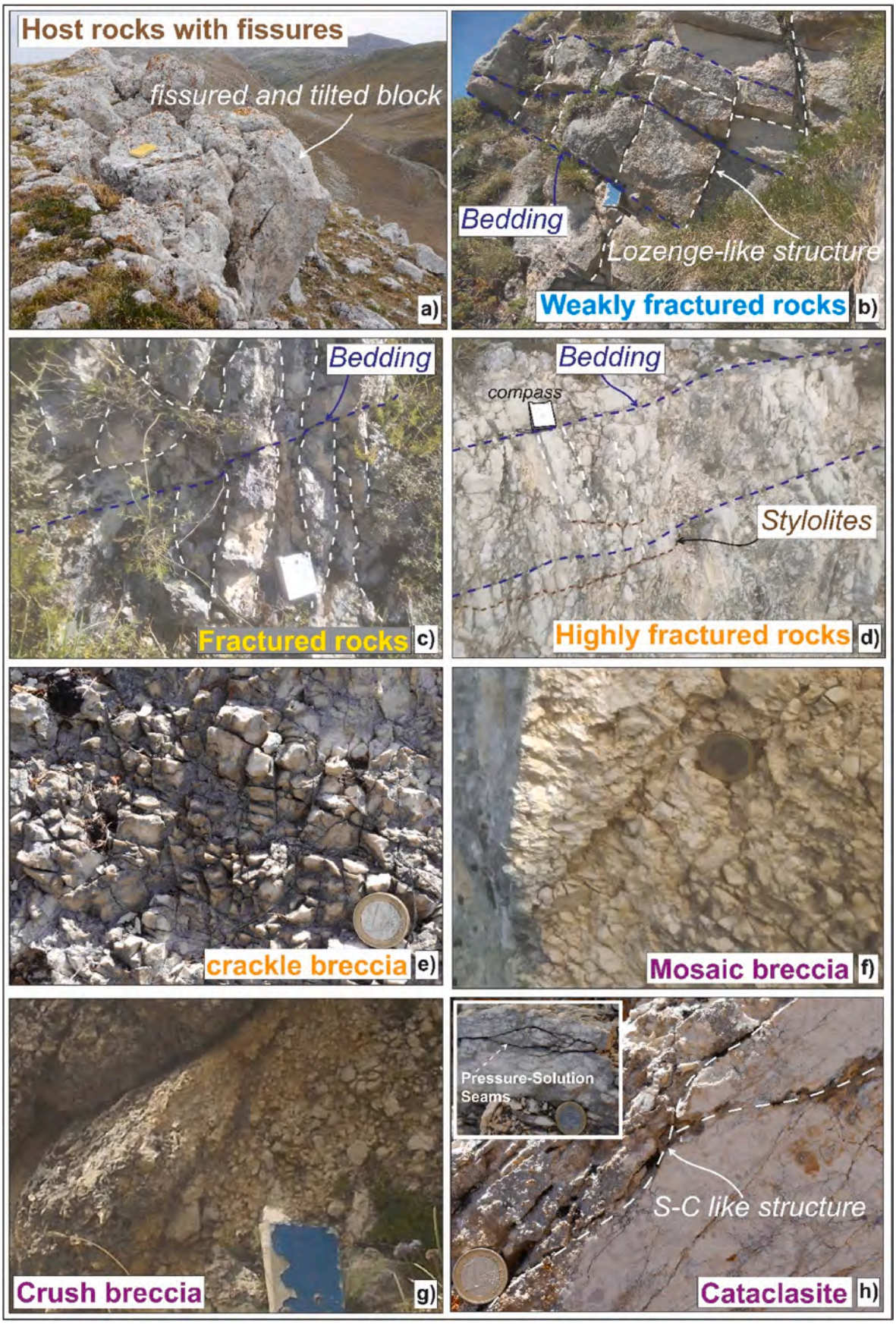

(caption on next page)

Fig. 3. Main structural units identified across the Campo Felice and Cama fault zones. a) Host rock with fissures, very large and locally causing the tilt of carbonate blocks down to the valley. b) Weakly fractured rocks, with high angle fractures (dotted white lines) forming lozenge-like structures. c) Fractured rocks affected by sub-vertical fractures spaced 3–10 cm apart. d) Highly fractured rocks, with subvertical fractures usually cut by stylolites striking sub-parallel with the bedding surfaces. e) crackle breccias, where fractures are spaced ~1 cm apart. f-h) Mosaic breccias, crush breccias and cataclasites, with pressure-solution seams and S–C like structures caused by pressure-solution processes. WGS84 GPS Location: 42.286720°N, 13.393950°E (a); 42.235224°N, 13.437680°E (b); 42.219666°N, 13.460662°E (c); 42.226981°N, 13.453245°E (d); 42.223688°N, 13.455338°E (e); 42.220531°N, 13.459215°E (f); 42.233561°N, 13.438081°E (g); 42.238451°N, 13.431004°E (h).

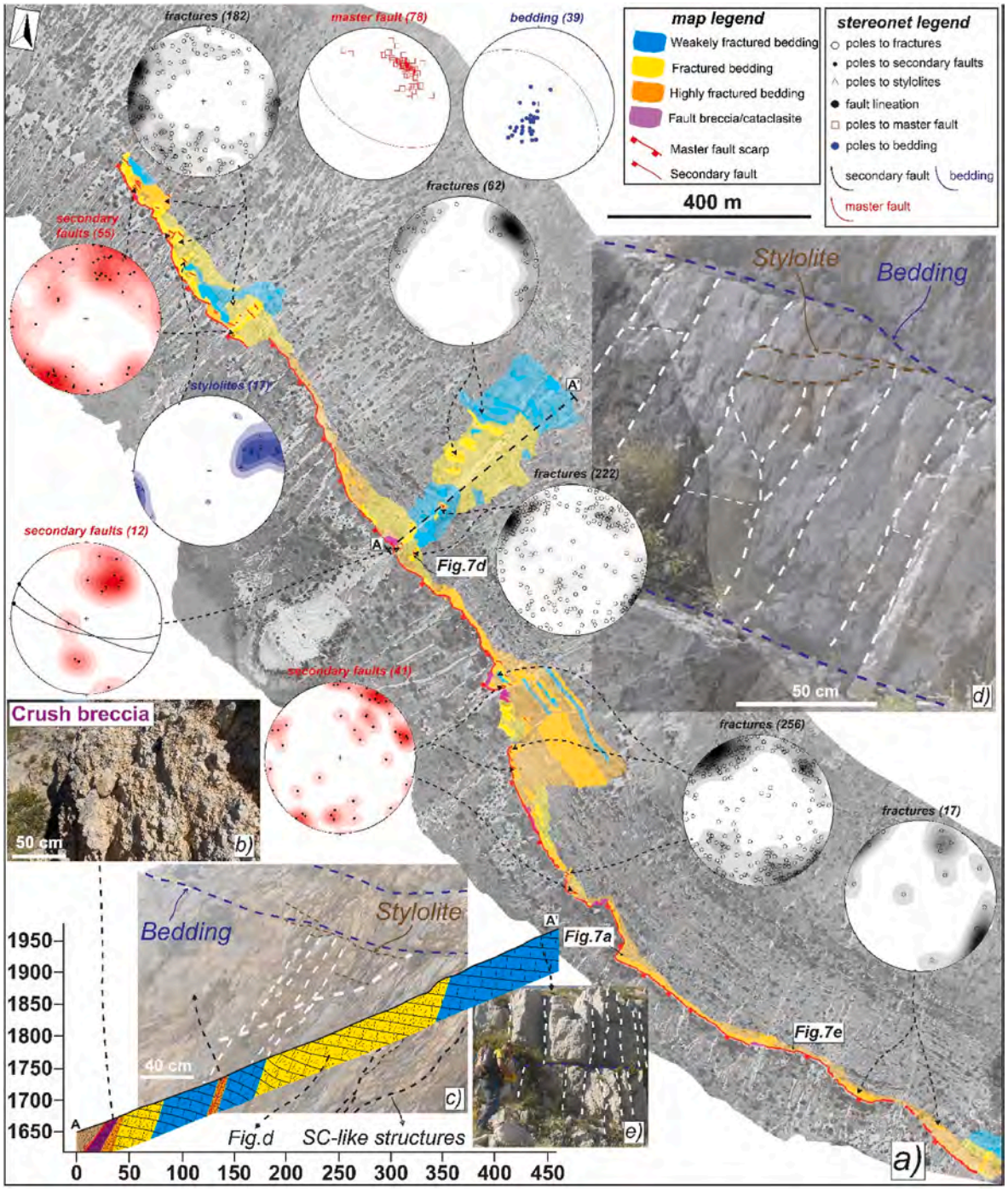

Fig. 4. a) Structural map of the Campo Felice fault zone in the Mt. Cefalone sector, cross-section (NE oriented) across the fault zone and structural data collected within the different structural units, plotted in Equal Area-Lower Hemisphere stereonets with density contours areas (see figure legend for symbols description). The inferred distribution of the structural units was drawn with higher degree of transparency. b) Fault core consisting of crush breccias. c) Highly fractured rocks, affected by high angle fractures (dotted white lines) spaced <3 cm apart, cut by lower angle fractures and bedding parallel stylolites, and locally forming S–C like structures. d) Fractured rocks, consisting of > 1-m-thick carbonate strata affected by high angle fractures spaced <10 cm apart, cut by stylolites. e) Weakly fractured rocks, cut by high angle fractures spaced >10 cm apart.

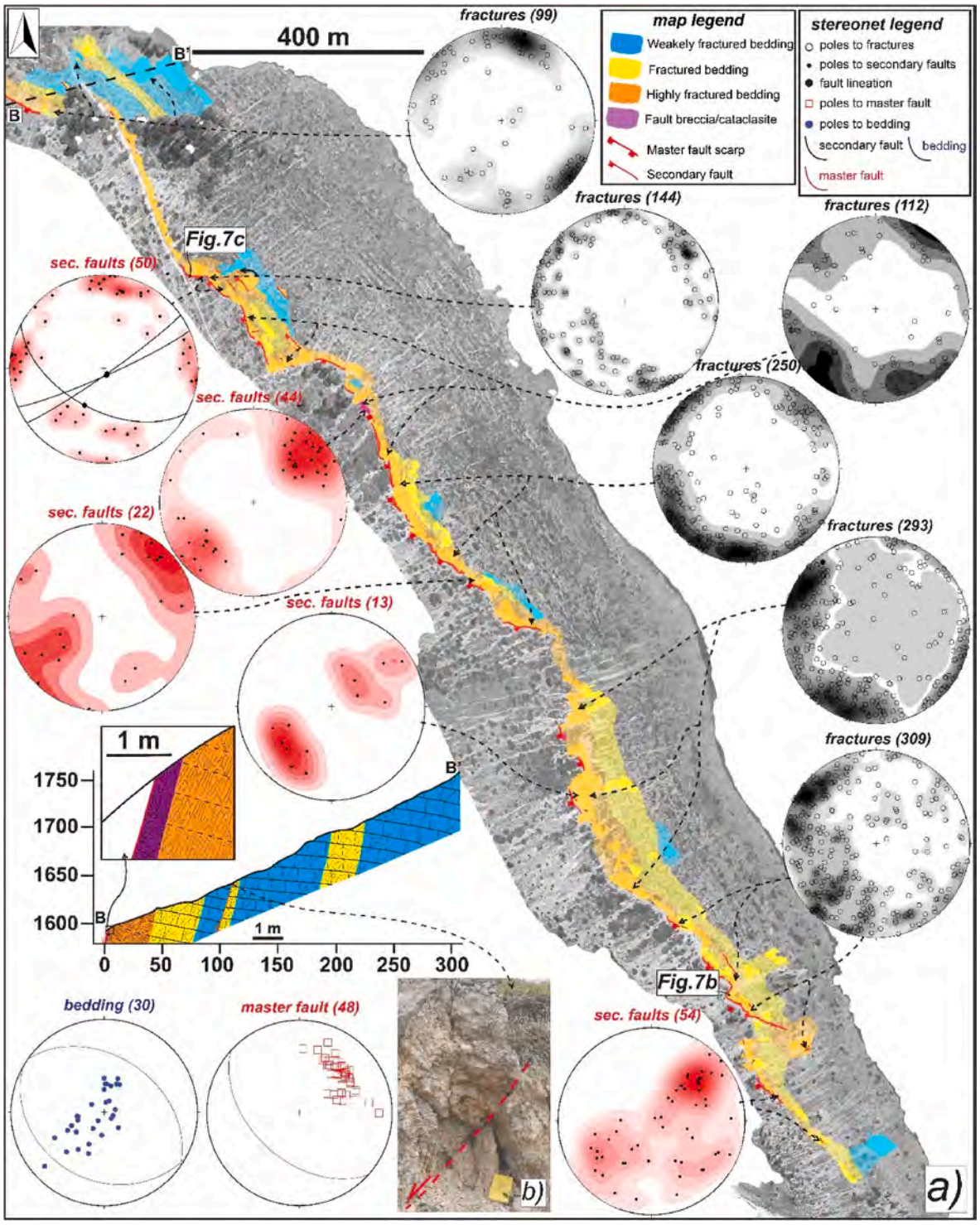

Fig. 5. a) Structural map of the Campo Felice fault zone in the Mt. Serralunga sector, cross section (ENE oriented) across the fault zone and structural data collected within the different structural units, plotted in Equal Area-Lower Hemisphere stereonets with density contours areas (see figure legend for symbols description). The inferred distribution of the structural units was drawn with higher degree of transparency. b) Detail of a large secondary fault affecting the host rocks in Fractured rocks domains, with a fault crush breccia associated.

structures (Fig. 3b).

Fractured rocks (yellow in the structural maps; e.g., Figs. 3–6) consist of fractured rock volumes, where bedding surfaces are still clearly recognizable and rarely cut by fractures. The latter are both sub-vertical (i.e., dip angle >65°) and sub-horizontal (i.e., dip angle <20°) with respect to the bedding surfaces and spaced 3–10 cm apart (Fig. 3c).

Highly fractured rocks (orange in the structural maps; e.g., Figs. 3–6) consist of highly fractured rock volumes, with strata partially recognizable (Fig. 3d). Extensional fractures are oriented both sub-vertical and at 40°–55° with the bedding surfaces, with 1–3 cm of spacing among fractures, or sub-horizontal, spaced 1–15 cm apart. Where fracture abundance increases (i.e., where both sub-vertical and sub-horizontal fractures are spaced ~ 1 cm apart), the highly fractured rocks appear as crackle breccias (i.e., incohesive fault breccia with

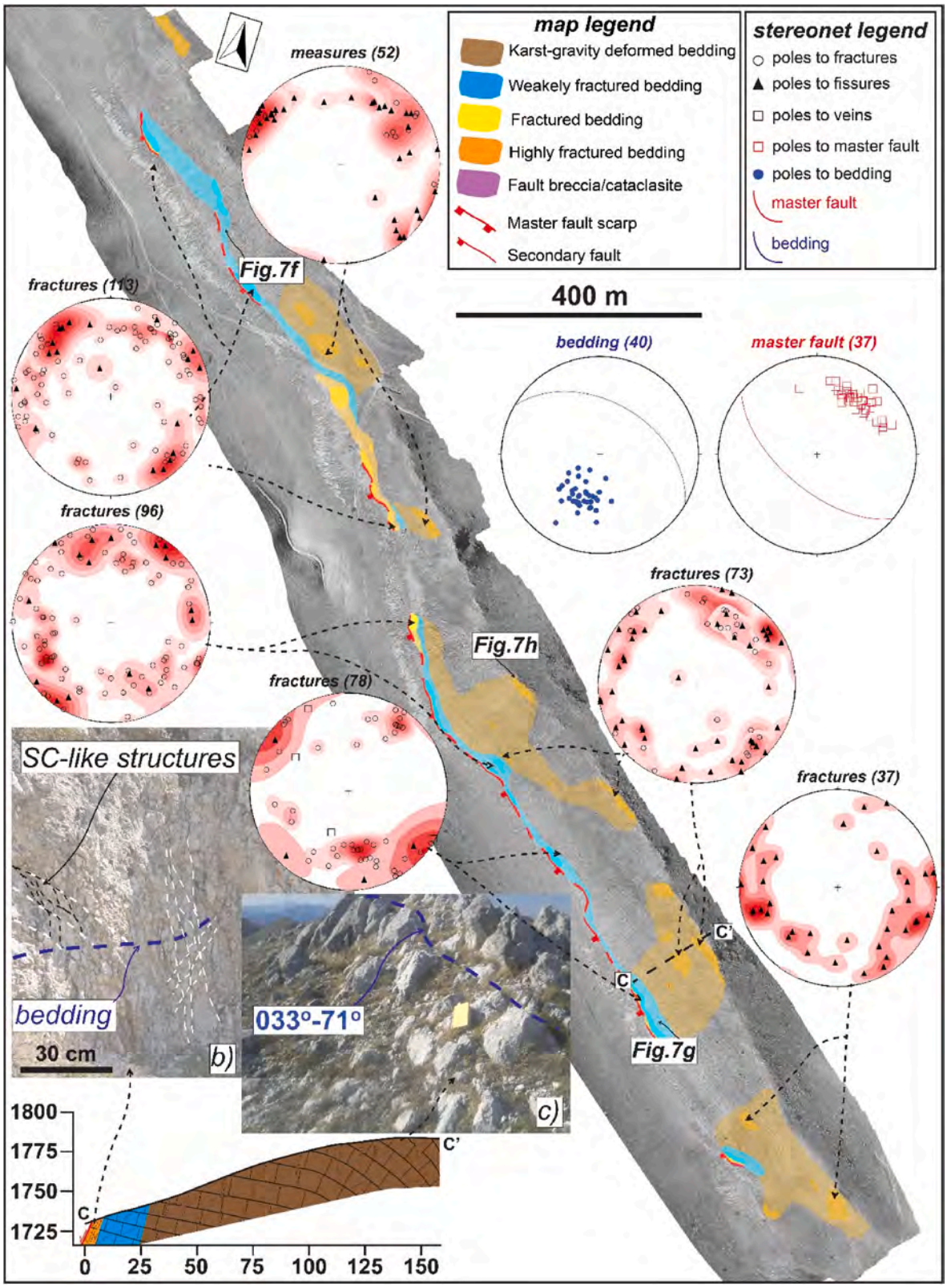

Fig. 6. Structural map of the Cama fault zone, cross section (NE oriented) across the fault zone and structural data collected within the different structural units, plotted in Equal Area-Lower Hemisphere stereonets with density contours areas (see figure legend for symbols description). The inferred distribution of the structural units was drawn with higher degree of transparency. b) Highly fractured rocks located close to the master fault scarp, with fractures spaced <3 cm apart and arranged in several sets, locally forming S–C like structures. c) Carbonate host rocks located close to the hill crest, dipping at high angles and affected by large fissures with 2–30 cm of aperture.

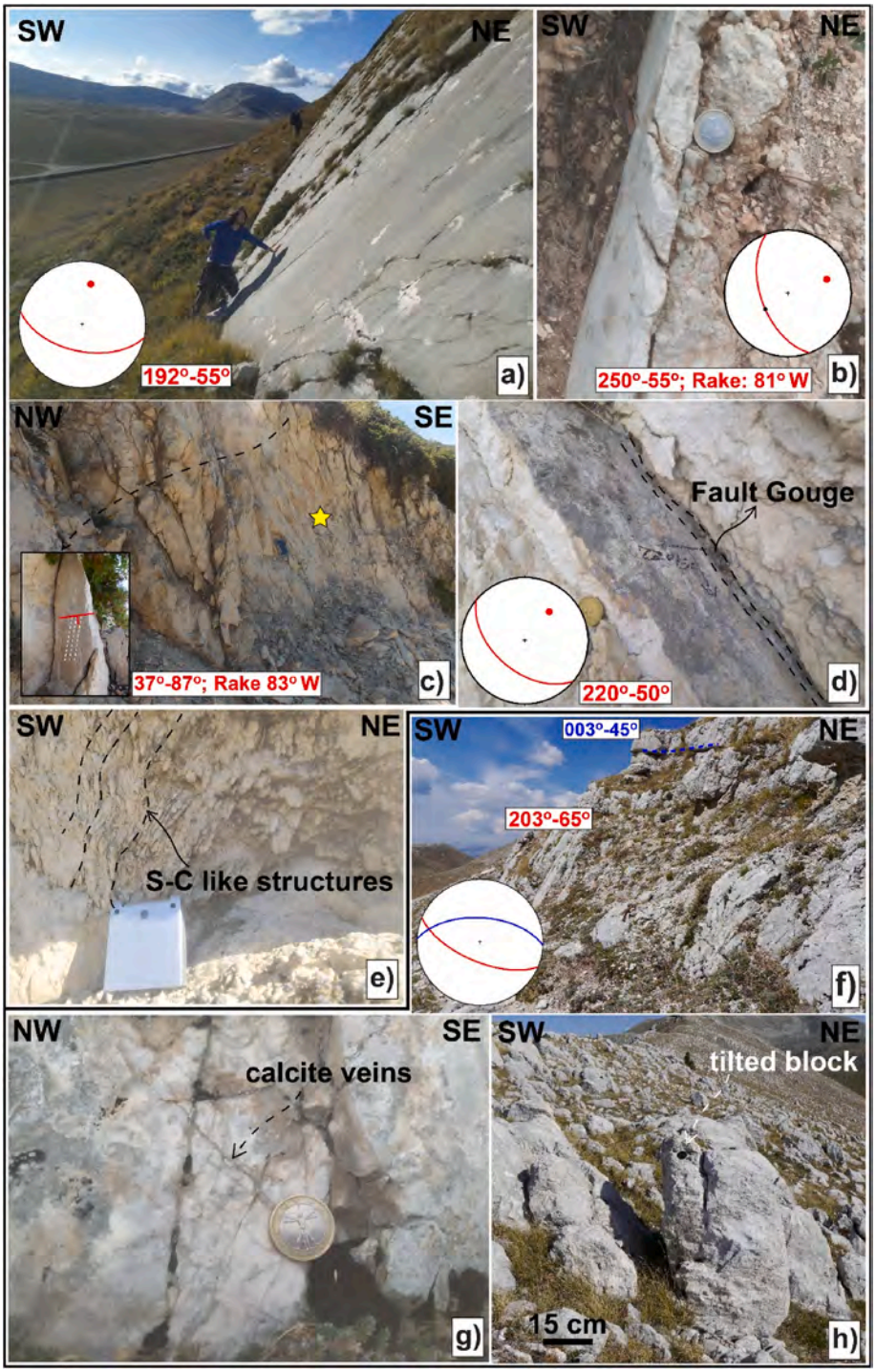

Fig. 7. Main structural elements observed in the Campo Felice and Cama fault zones. a) Campo Felice fault scarp along the Mt. Cefalone, reaching the maximum height of ~15 m. b) Polished Campo Felice fault surface affecting the bauxites (Sample CF22_P). c) Cataclastic fault core in between a step-over zone affected by numerous secondary faults with polished slip surfaces showing a dip-slip kinematics (Star indicates the location of Sample CF05). d) Large secondary fault with gouge associated, dipping synthetically with the master fault. e) S–C like structures in Highly fractured volumes across the Campo Felice fault zone. f) Cama fault scarp sharply cutting NE dipping carbonate rocks. g) Small and thin calcite veins, conjugated themselves, affecting the karstified Cama fault surface. h) Blocks of carbonate host rocks close to the hillcrest top cracked and tilted down to the slope. Red and blue lines in the stereoplot indicate the fault and bedding attitude, respectively. WGS84 GPS Location: 42.227594°N, 13.445696°E (a); 42.212690°N, 13.466460°E (b); 42.223827°N, 13.454746°E (c); 42.234210°N, 13.437396°E (d); 42.227505°N, 13.447607°E (e); 42.274730°N, 13.411760°E (f); 42.275030°N, 13.411420°E (g); 42.278070°N, 13.408900°E (h). (For interpretation of the references to color in this figure legend, the reader is referred to the Web version of this article.)

>75% of clasts >2 mm; Woodcock and Mort., 2008, Fig. 3e). Highly fractured, Fractured and Weakly fractured rocks represent the footwall damage zone of the studied fault zones. Highly fractured and Fractured rock volumes usually crop out close to or few meters away from the master fault surface or in areas strongly affected by secondary faults.

Cataclasite/Breccias (purple in the structural maps; e.g., Figs. 3–6) consist of crush breccias and incohesive mosaic breccias composed of angular host-rock-built fragments (~5 mm–10 cm and ~5 mm to 2 cm in size, respectively) surrounded by a fine matrix (~10% of total volume; sensu Woodcock and Mort., 2008, Fig. 3f and g) and cohesive fault rocks with ultra-cataclastic (i.e., >90% of fine calcite matrix), cataclastic (i.e., 90-50% of fine matrix; Fig. 3h) or proto-cataclastic fabrics (i.e., 50-10% of fine matrix). In these volumes, bedding surfaces and other sedimentary structures (e.g., stromatolitic laminations or "burial" stylolites/pressure-solution seams) are not recognized.

4.2.1. *The Campo Felice fault*

The Campo Felice master fault is exposed along the western slope of Cefalone and Serralunga Mts. with a ~5.8-km-long fault scarp (Figs. 4 and 5). The fault scarp has an average height of about 3–4 m (up to 15 m in some sectors; Fig. 7a) and crops out almost continuously along Cefalone Mt., whereas it is less continuous and wavier along-strike along Serralunga Mt. (Figs. 4 and 5). The exposed fault surface is very sharp, but also strongly karstified, except in the south-eastern tip. Here, in the

areas where the fault cuts the bauxitic levels, the fault surface is locally well preserved and appears very polished (Fig. 7b). The fault dips 45°–75° (mean dip angle of 55°) to SW and sharply truncates the carbonate host rocks, dipping 5°–50° to NW (see stereonets in Figs. 4–5). In contrast, along the numerous left-stepping transfer zones, the master fault surface dips to SSW-SE and the host rocks dip towards SW in the relay ramp (see bedding and master fault stereonets in Figs. 4 and 5).

Fracture abundance increases close to the master fault and within the step-over zones, where the fault core and Highly fractured rocks crop out. The fault core units mainly consist of (i) cataclasites with white to reddish matrix (<40-cm-thick, up to 3-m-thick in the step-over zones; Figs. 3h and 7c) and (ii) fault breccias (Figs. 3g and 4b), commonly 50-cm- to 2-m-thick, up to 5-15-m-thick in the master fault step-overs and bends (see cross-section A-A' in Fig. 4). Highly fractured volumes crop out close to either the master fault or the fault core with a thickness of 15–150 m. Both Highly fractured and cataclastic rocks are cut by calcite-bearing veins and by numerous steeply dipping (60°–90°) secondary faults (Figs. 5b and 7d) that mainly strike NW-SE and dip both synthetically (i.e., with similar dip azimuth) and antithetically (i.e., with opposite dip azimuth) with respect to the master fault (see stereonets in Figs. 4 and 5). In the fault core, minor secondary fault surfaces also strike N and E. Where the fault surfaces are very polished, the kinematic indicators show a normal dip-slip and rarely strike-slip kinematics (Figs. 5 and 7c). In the central sector, extensional fractures are arranged in several sets striking from SSE to NE and from N to S, consistent with the orientation of the secondary faults (Figs. 4 and 5). Most of the fractures are oriented at high angle (i.e., 60–90°) with respect to the bedding surface and are usually cut by fractures with 40°–55° of dip angles (Figs. 3d and 4c).

Fracture abundance within the damage zone slightly decreases towards the master fault tips (i.e., average fracture spacing >3 cm), particularly in the north-western sector, where Fractured rock volumes (Fig. 3c) are more abundant, but still affected by numerous secondary faults (Figs. 4 and 5). Here, the fractures mainly dip from SE to NW both at high (i.e., >65°) and low angles (i.e., <35°) without cutting the bedding surfaces (Figs. 3c, 4-5). High angle fractures are spaced 3–10 cm apart and usually cut the low angle ones, spaced up to 1 m apart (Fig. 4d). Fracture intensity drastically decreases ~60–120 m away from the master fault surface, where the host rocks are cut by sub-vertical fractures spaced >10 cm apart and are not affected by secondary faults (Figs. 3b and 4e). Fractured rocks usually represent the transition unit between Highly (Fig. 3d) and Weakly fractured domains (Fig. 3b), although sharp contacts between these two units were also observed, due to the presence of a large secondary fault or an abrupt change in the thickness of the carbonate strata (i.e., from ~1 m to 20–30 cm).

The fault core (~15-m-thick) and damage zone units extend for >400 m across a large incision feeding the fan located in the middle sector of Mt. Cefalone (see cross-section A-A' in Fig. 4). In this area, the abundance of fractures affecting the host rocks gradually decreases (i.e., from <1 cm to >10 cm of fracture spacing) up to ~ 150 m away from the master fault. Then, Fractured rocks (Figs. 3c and 4d) crop out across the incision for ~160 m, after which less fractured volumes are exposed. In the latter, the fractures are spaced 15–30 cm apart and dip sub-vertically (dip angles of 65°–90°) towards SW and NE cutting > 1-m-thick carbonate strata (Fig. 4e). In both fault core and damage zone, pressure-solution processes result in the formation of seams and stylolites striking parallel to the bedding strata, usually cutting calcite veins and subvertical fractures and locally displaced by fractures oriented at 40°–55° with the bedding surfaces (Figs. 3d and 4c, d). Furthermore, in both the fault core and Highly fractured domains, pressure-solution also allow the development of S–C like structures at different scales (e.g., Figs. 3h, 4c and 7e).

4.2.2. The Cama fault

The Mt. D'Ocre range is composed of three NW-SE oriented fault branches spreading from Mt. D'Ocre, to SE, to the Campoli Basin, to NW (Fig. 1b). The Cama fault represents the south-western branch of the Mt. D'Ocre range. Our fieldwork surveys were conducted along this fault because of the very sporadic outcrops of the major scarp and footwall host rocks associated with the larger Campoli-Cerasitto fault (Fig. 1b). The Cama fault is ~3.4-km-long and borders the Cama Valley in the north-western sector and Vallefredda and Santo Lago Valleys in the middle and south-eastern sectors, respectively (Figs. 1c, 2b and 6). The fault scarp crops out mainly in the middle and southern sectors (maximum height of ~2 m), although discontinuously (Fig. 6). The scarp dips 49°–70° (~60° on average) to SW and affect the same carbonate rocks in the footwall of the Campo Felice fault. The host rocks dip to N-NE with 20°–45° of dip angles up to 100 m away from the master fault scarp (Fig. 7f) and with 50°–70° of dip angles close to the hill crest (Fig. 6c).

Both the fault core and the damage zone crop out for a total thickness <40 m. The fault core crops out only close to the south-eastern tip, where it is ~ 1-m-thick and mainly consist of crush breccias, whereas Highly fractured (Fig. 6b) and Fractured rocks (up to 15–30 m in thickness) are mainly distributed in the area located between Vallefredda and Santo Lago Valleys. In these domains, none secondary fault was observed and only few calcite veins (<4 mm thick) associated with the major scarp, mostly arranged in conjugate systems, were mapped (Figs. 6 and 7g). Mode I fractures are mainly oriented at high angles with respect to the bedding surfaces and largely scattered in dip attitude, forming different sets usually conjugated themselves (Fig. 6). As in the case of Campo Felice fault, in the few areas close to the master fault in which the spacing among fractures is less <3 cm, pressure-solution processes contribute to the formation of S–C like structures (Fig. 6b).

Where the damage intensity decreases along the master fault, 15-to-35-m-thick Weakly fractured domains (Fig. 3b) crop out, with both sub-vertical (i.e., dip angles of 60°–90°) fractures and fissures (<2 cm of aperture) spaced >10 cm apart. Outside the damage zone, starting from ~40 m to the NE from the master fault surface till the hillcrest top, the host rocks are almost undeformed and only affected by high angle sub-vertical fractures and fissures (1–20 cm of aperture) spaced 20 cm to 1 m apart and with scattered dip attitude (i.e., Host rocks with fissures domain; Figs. 3a and 6). In this sector, the bedding and fracture/fissure surfaces are very rough, possibly due to karst processes (Figs. 3a and 6). Moreover, moving up to the hillcrest top, most fissured blocks are tilted by gravity towards the valley slope (Figs. 3a and 7h).

4.3. Microstructures of the slip zones

In this section, we describe the microstructures of the slip zones of the Campo Felice and Cama faults following the classification of Sibson (1977, 2003). We define as slip surface the exposed fault surface, either polished or karstified. We indicate as slip zone the deformed rocks located beneath the slip surface (up to several centimeters thick) that accommodate the shear strain produced during fault slip (Chester and Chester, 1998; Sibson, 2003). Where present, Principal Slip Zones (PSZs) consist of texturally distinct layers, usually few mm thick, located immediately beneath the slip surface, that accommodate most of the fault displacement (Smith et al., 2011).

4.3.1. Slip zones of the Campo Felice fault zone

The slip zone associated with the Campo Felice master fault surface (mostly rough, due to karst-erosional processes) has a proto-cataclastic fabric consisting of angular to sub-rounded fragments of the host rocks (1–5 mm thick) surrounded by a fine matrix (white or reddish in the field and dark grey or brownish under the OM; Fig. 8a). Moving toward the slip surface, the fabric becomes more cataclastic, as the amount of fine matrix increases up to >50% of the total volume (Fig. 8a). The fragments are cut by numerous shear fractures (<0.5 mm thick) oriented sub-parallel (i.e., Y-shear fractures) or up to ~ 40° with respect to the slip surface (i.e., P-shear fractures). Some of them are filled with calcite (see black arrows), oxides or clay minerals (Fig. 8a–d). Where clay minerals

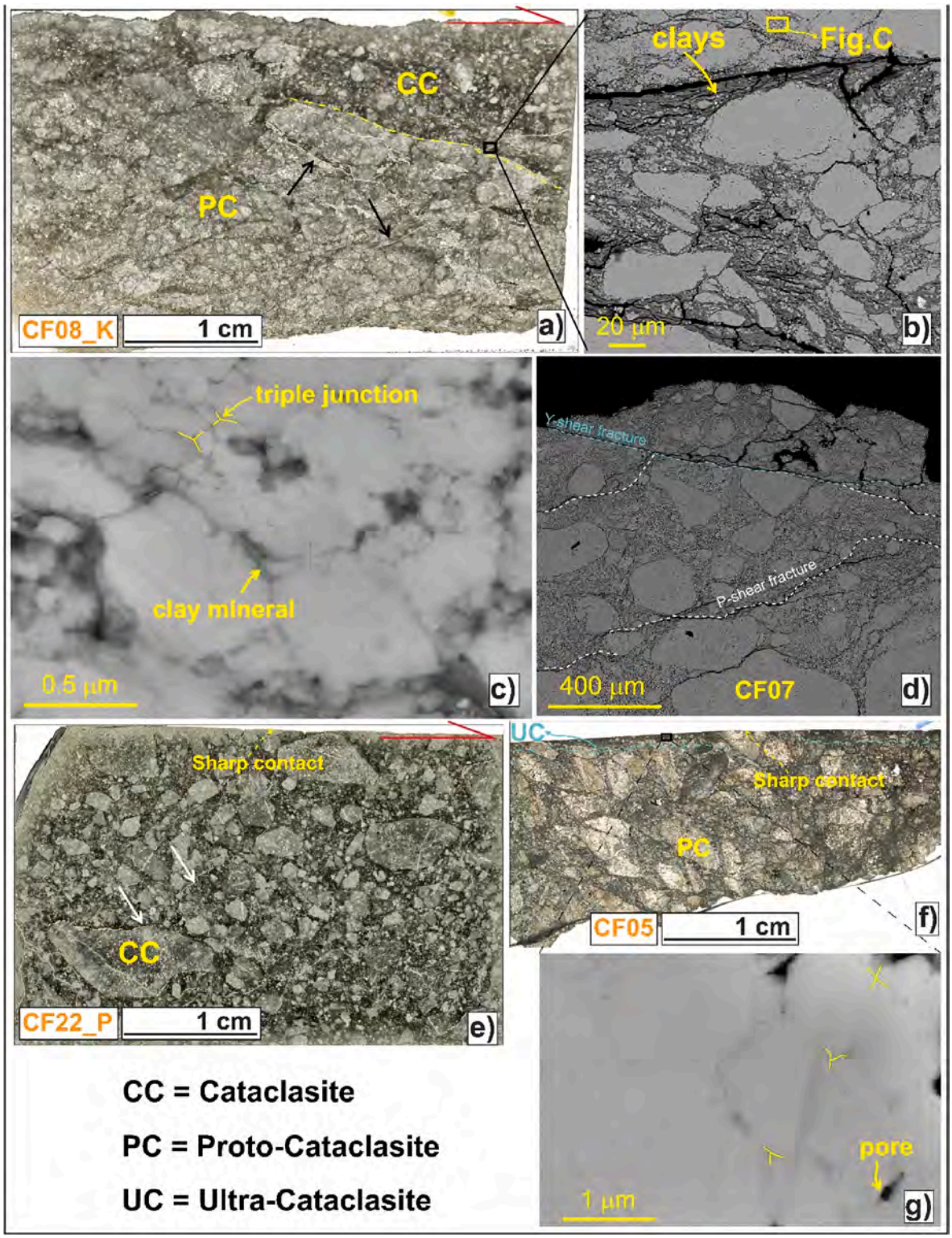

Fig. 8. Microstructures of the slip zones of the Campo Felice fault zone. a) Slip zone associated with the master fault surface (quite rough), showing a proto-cataclasitic to cataclasitic fabric made of angular to sub-rounded host rock fragments (1–5 mm thick) immersed in a fine grey matrix and cut by < 0.5-mm-thick fractures filled with calcite (black arrows). b-c) Clay minerals filling the fracture spaces and surrounding the calcite grains. The latter shows stylolitic-like boundaries and from incipient triple junctions. d) Y-shear and P-shear fractures close to the slip surface. e) Well-preserved slip surface, very smooth and with a net contact with the calcite fragments, partially rimmed by < 0.5-mm-thick calcite veins (black arrows). f) Slip zone of a well-preserved minor fault including a discontinuous ultra-cataclastic layer (i.e., PSZ) close to the polished slip surface, that has a net contact with the calcite fragments. g) Matrix of the PSZ, composed of sub-euhedral calcite grains with straight boundaries, forming well-developed triple and quadruple junctions. WGS84 GPS Location: 42.227594°N, 13.445696°E (a, b, c, d); 42.212690°N, 13.466460°E (e); 42.223827°N, 13.454746°E (f, g).

and oxides are abundant, the texture of fine matrix is composed of calcite micro-grains with irregular to stylolitic-like boundaries, commonly indented and forming incipient triple junctions, with numerous pore spaces locally filled with clay minerals (Fig. 8b and c). Where the fault surface is locally preserved along-strike by sub-aerial exposure, the slip surface is very smooth and has a sharp contact with the underlying clasts (Fig. 8e). The slip zone is a well-developed cataclasite composed of millimeters to centimetres in size sub-angular fragments cut and locally rimmed by thin veins filled by sparite and oxides (white arrows in Fig. 8e).

The minor secondary faults affecting the fault core in the step over zones have a very smooth slip surface and a slip zone made of angular to sub-rounded fragments. The latter are 2–8 mm in size, are internally fractured and are immersed in a dark fine matrix (<50% of the total volume; Fig. 8f). The slip zone includes also a ~ 1-2-mm-thick discontinuous ultra-cataclastic layer close to the slip surface, made of >90% of fine matrix surrounding few rounded clasts (<0.5 mm in size; Fig. 8f). The matrix shows a foam-like fabric consisting of sub-euhedral micrometric to nanometric in size calcite grains with straight boundaries, forming triple and quadruple junctions and few pore spaces (Fig. 8g).

4.3.2. *Slip zones of the Cama Fault zone*

The fault rock close to the Cama fault surface is a chaotic to mosaic breccia (Woodcock and Mort, 2008) composed of incipient angular clasts (1–10 mm in size) cut by numerous fractures oriented 50°-90° to the slip surface (very rough due to karst processes) and forming conjugated pairs (Fig. 9a). Most fractures are filled with secondary sparite, composed of blocky and almost euhedral calcite grains (Bons et al., 2012), with straight and indented (white in color arrows in Fig. 9d) boundaries (Fig. 9c and d).

In the few and small (i.e., 2–5 m along-strike) areas where the intensity of damage increases along the fault scarp, the slip zone consists of <1 mm–5 mm in size sub-angular clasts surrounded by a brownish fine matrix (Fig. 9b). The slip zone includes numerous pores and fractures oriented both at high-angle and parallel to the slip surface, rarely filled with calcite, and thin convoluted layers close to the top. Overall, this fabric is quite similar to the one observed in the slip zone of the Campo Felice fault (Fig. 8a–e).

5. Discussion

In section 5.1 we discuss the structural features associated with the Campo Felice and Cama normal fault zones, affecting the same carbonate rocks with different cumulated throws (Table 1). In section 5.2 we interpret the main the deformation mechanisms active during sliding in the fault slip zones (Table 1). We further discuss the geomorphological evidence supporting the hypothesis that currently the Cama normal fault represents the upper emergence of the basal shear zone associated with the lateral spreading (DSGD) of Mt. D'Ocre Range. In fact, as for most of the lateral spreading DGSDs, the basal shear zone does not crop out (Varnes, 1978; Hutchinson, 1988; Agliardi et al., 2001, 2012; Dramis and smile-valvo, 1994; Discenza and Esposito, 2021).

5.1. *Macro-structural proprieties of the Campo Felice and Cama faults*

The Campo Felice fault has an almost continuously exposed sharp fault scarp ~ 3-4-m-high on average, up to 15 m in some areas (e.g., Fig. 7a), locally undulated along-strike (Figs. 4–5). The fault core decorates the fault scarp for several kilometres and mainly consists of cataclasites (~0–40 cm in thickness) and crush fault breccias (50-cm to 2 m

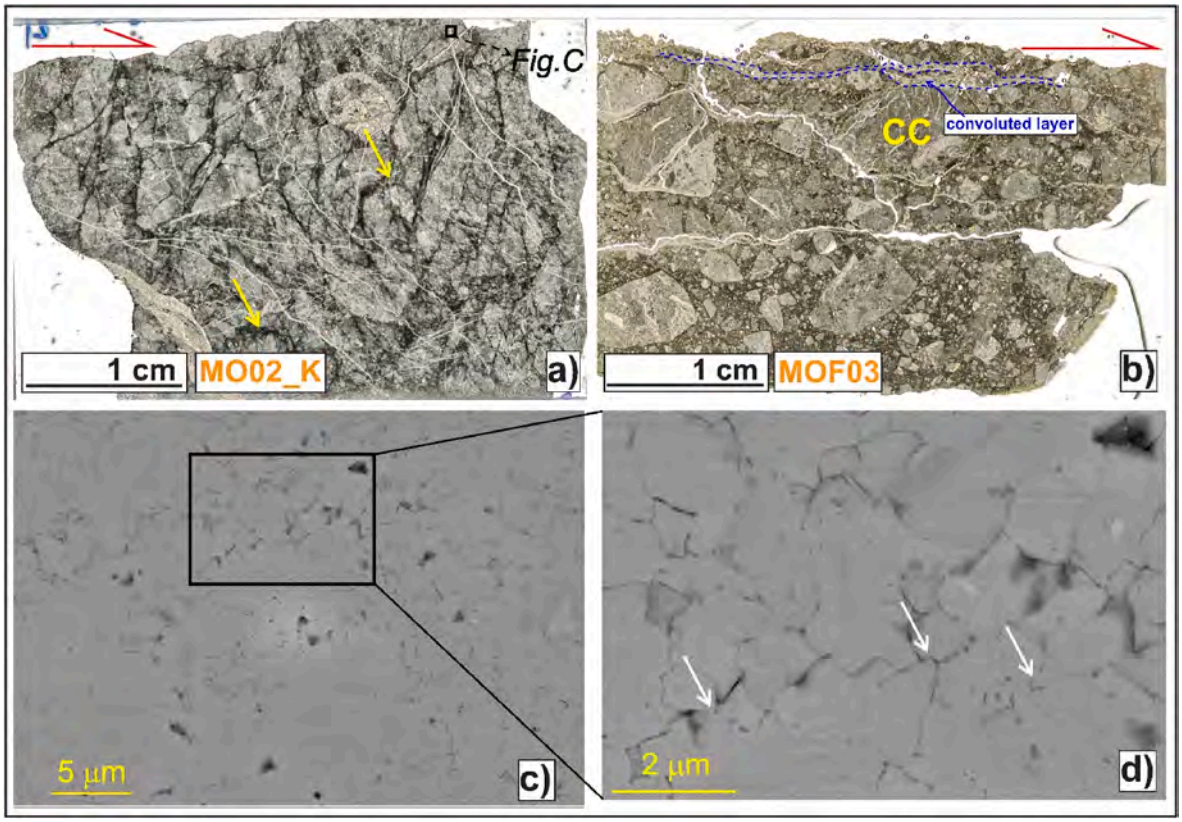

Fig. 9. Microstructures of the Cama fault slip zone. a) The slip zone consists of chaotic to mosaic breccias composed of <1 cm in size angular clasts, cut by numerous fractures oriented at high angles with the very rough slip surface, locally filled with sparite. b) Slip zone where the intensity of fractures increases, showing a cataclastic fabric composed of sub-angular clasts with different size surrounded by a fine matrix and cut by large fractures oriented both at high-angles and parallel to the slip surface (very rough due to karst processes). c-d) Blocky calcite grains filling the fracture spaces, with straight to indented boundaries (white arrows). WGS84 GPS Location: 42.275030°N, 13.411420°E (a, c, d); 42.283250°N, 13.398110°E (b).

Table 1
Comparison of the main geological and structural features of the Campo Felice and Cama faults.

Properties	Campo Felice fault	Cama fault
Along-strike length	~6 km	~3 km
Fault scarp height	~4 m, up to 15 m	max. 2 m
Max. geological throw	1050 (425 m of possible overestimation)	~100 m
Throw rates	~1 mm/yr	0.2 mm/yr
Damage zone thickness	>400 m	~40 m
Core thickness	~40 cm, up to 15 m	Almost absent
Secondary faults	Tens to hundreds in both core and damage zone	not found
Veins	Tens to hundreds in both core and damage zone	Close to the fault scarp and thick <5 mm
Slip zones microstructures	Cataclasite to Ultra-Cataclasite	Crush breccia to cataclasite
Deformation mechanisms	Cataclasis and pressure-solution	Cataclasis and pressure-solution

in thickness). The latter are cut by calcite veins and several sub-vertical secondary faults dipping both synthetically and antithetically with the master fault and controlling the heterogeneous distribution of the different structural units forming the footwall damage zones (Fig. 3b–e). In particular, Highly fractured and fractured rock volumes are spatially associated with secondary faults. In these domains, most of the fractures are spaced <3 cm and 3–10 cm apart and steeply dipping, with orientation consistent with the one of the secondary faults and with the ongoing NE-SW oriented Pleistocene regional extension (Ferrarrini et al., 2015; Lavecchia et al., 1994). The fault is composed of numerous segments arranged in én-echelon step-over zones, where the fault core is wider (i.e., up to 15-m-thick) and fracture intensity strongly increases, thus favoring the infiltration of meteoric waters and the development of stylolites and S–C like structures (Fig. 3a, 6c-d, 7e). Such structural features were also observed in other large-displacement normal faults in the central Apennines (e.g., San Benedetto-Gioia dei Marsi fault segment, Agosta and Aydin, 2006; Campo Imperatore fault system, Fondriest et al., 2020; Demurtas et al., 2016) although these faults have wider fault cores (i.e., 1–40 m thick) and damage zones (up to several hundred meters thick).

Instead, the architecture of the Cama fault is less structurally developed compared with the one of Camo Felice fault. The fault scarp is discontinuous and crops out only in the middle and southern sectors, with maximum height of ~2 m. The fault core is almost absent, except close to the south-eastern tip, where it consists of mosaic fault breccias (Woodcock and Mort, 2008) and the damage zone is < 40-m-thick and not affected by secondary faults (Fig. 6). Extensional fractures are usually spaced >10 cm apart, except in few areas close to the master fault, where they are spaced <3 cm apart and conjugated themselves (Fig. 6) with orientation consistent with the Pleistocene extensional phase. These architectural features are typical of immature/incipient or small-displacement faults (Faulkner et al., 2011; Savage and Brodsky, 2011; Mayolle et al., 2019) and would be consistent with the ~100 m of maximum geological throw (cross-section B–B'; Fig. 2d) and low Quaternary throw rates estimated (0.2 mm/yr; Salvi et al., 2003).

This interpretation would be also confirmed by the absence of wide (i.e., tens of kms^2) Quaternary basins associated with the Monte D'Ocre faults, that instead border small and narrow (i.e., <400 m wide; Figs. 1, 2 and 6) valleys to SW. Indeed, large Quaternary basins are commonly associated with tens of km-long active normal faults, especially in central Apennines (Bosi et al., 2003), where, however, some basins could have been inherited from the compressional stage (e.g., in between nearby thrusts) and not directly produced by the bounding normal faults (Mancinelli et al., 2021).

Nevertheless, several sub-vertical fissures affect the host rocks in the footwall of the Cama fault. Average fracture/fissure aperture increases from 10 to 15 cm to >20 cm (up to 1 m) toward the hillcrest top, also favored by dissolution associated to karst processes, that are very efficient in calcite-built rocks especially at low ambient temperature (Andriani and Parise, 2015). Here, the relatively high potential relief promotes the formation of gravitational trenches, that are commonly associated with tilted blocks at the surface (Figs. 3a and 7h). Other landforms typically associated with gravitational processes, such as double-crested lines, up-hill and down-hill facing scarps, mainly aligned in the NW-SE direction, shape the Mt. D'Ocre range (see Fig. 2 in Albano et al., 2015; Salvi et al., 2003, Fig. 1). The large fissures affecting the host rocks and associated landforms are consistent with their development in tensional regime (i.e., negative values of minimum principal stress; Del Rio et al., 2021) or at very low confining pressures, with principal stress oriented sub-parallel to the fracture surface (i.e., Mode I fracture; Fossen, 2010). These structural and geomorphological observations suggest that the Cama master fault surface is currently accommodating the lateral spreading of Mt. D'Ocre Range, mainly moving by creep, together with the Campoli-Cerasitto fault and other faults of the area (Figs. 1 and 2b, d). Therefore, this fault is not expected to link at depth with the Campo Felice fault, given the large differences in cumulated throw and throw rates (Table 1) and the current mechanical behaviors (i.e., tectonic vs. gravitative) and, thus, not represent a segment of the active Ovindoli-L'Aquila Fault System as proposed by other authors (Salvi et al., 2003; Galli et al., 2008). However, given the proximity with the Campo Felice fault, episodic movements along these faults can likely be induced by ground shaking produced by earthquakes (Salvi and Nardi, 1995; Albano et al., 2015), also consistent with the average fault dip angles of ~60° (Fig. 5). According to this interpretation, the length of the seismogenic source associated with the Ovindoli-L'Aquila Fault System would be reduced of ~ 8–9 km. This, in turn, would result in a lower maximum expected earthquake magnitude (i.e., M_w ~ 6.5) associated with the entire re-activation of the fault system (e.g., Wells and Coppersmith, 1994; Wesnousky, 2008; Leonard, 2010; Galli et al., 2008).

5.2. *Deformation mechanisms of the Campo Felice and Cama fault slip zones*

In active fault zones, the bulk of displacement cumulated during individual earthquakes is mainly accommodated in the fault core, in particular within highly localized cataclastic mm-cm thick principal slip zones (Power and Tullis, 1989; Chester et al., 1993; Caine et al., 1996; Chester and Chester, 1998; Sibson, 2003; Smith et al., 2011, 2015).

The Campo Felice fault surface is quite rough where the exposed fault scarp is karstified (Fig. 8a). The associated slip zone shows a proto-cataclastic to cataclastic fabric, including thin calcite veins and both Y-shear and P-shear fractures, but lack of a well-defined ultra-cataclastic layer close to the slip surface (i.e., the PSZ), possibly obliterated by weathering (Fig. 8a, d). Where preserved by surficial alteration, the fault surface is smoother and has a sharp contact with the larger clasts of the underlying cataclastic slip zone (Fig. 8e). The well-preserved slip surfaces of secondary faults are very smooth to polished, with an associated proto-cataclastic/cataclastic slip zone that includes a ~ 1-2-mm-thick ultra-cataclastic PSZ (Fig. 8f). On the contrary, the slip surface of the Cama fault is very rough, in part due to weathering of the exposed fault scarp, and lacks of a neat PSZ. Indeed, the fault rock beneath the slip surface is a chaotic to mosaic fault breccia cut by numerous fractures and calcite veins (0.1–0.2 mm thick) oriented at high-angles (i.e., >50°) with respect to the slip surface (Fig. 9a).

The fine matrix surrounding clasts in the Campo Felice master fault core is composed of calcite micro-grains with irregular to stylolitic-like boundaries, pores, incipient triple junctions and indentation structures interpreted as due to pressure-solution processes (Rutter, 1983; Gratier et al., 2013, Fig. 8b and c). Pressure-solution is a water-assisted process mainly driven by the stress acting at the grain-to-grain contacts that occurs through dissolution at grain boundaries, diffusion of the solute

matter, and precipitation of the latter within pore spaces (Rutter, 1983; Tada and Siever, 1989; Lehner, 1995; Gundersen et al., 2002; Croizè et al., 2013). Pressure-solution processes are locally promoted by the presence of oxides and clay minerals within the pore spaces, that prevent grain boundary healing (Renard et al., 2001), possibly deriving by the smearing of the bauxitic layers cut by the Campo Felice fault.

These processes are also controlled by the grain size (Rutter, 1983; Tada and Siever, 1989; Renard et al., 2000). Indeed, in the ultra-cataclastic PSZ, where the average grain size is smaller due to the higher degree of grain comminution, the fine matrix is mainly composed of more packed sub-euhedral calcite grains, with straighter boundaries and more developed triple junctions (Fig. 8g). Pressure-solution processes also favor dissolution and formation of stylolites (Ehrenberg et al., 2006; Aharonov and Katsman, 2009). In the case of Cama fault slip zone, the sub-grains of the fault breccia have irregular to stylolitic boundaries and are affected by numerous veins filled with secondary sparite (Fig. 9a). The latter is composed of sub-euhedral and blocky calcite grains with straight contacts and indentation structures suggesting fluid circulation and rapid precipitation after fracturing at very shallow crustal levels and congruent pressure-solution processes (Fig. 9c and d).

Microstructural analyses indicate that similar deformation mechanisms (i.e., cataclasis and pressure-solution) occur in both the Campo Felice and Cama faults. However, the slip zones associated with the two fault scarps have different fabrics (i.e., cataclasite *vs.* crush fault breccia) and textures of the fine matrix. These differences can be mainly explained by the higher average long-term slip rates and cumulated geological throws of the Campo Felice fault with respect to the Cama fault and also by the higher amount of clay minerals in the Campo Felice slip zone than in the Cama one (see Table 1). Indeed, in the few areas where the intensity of fracture increases along the Cama fault, the slip zone shows a cataclastic fabric quite similar to the one observed in the slip zone of Campo Felice fault (compare Fig. 8a–e, with Fig. 9b).

6. Conclusions

In this work, we compared the Campo Felice and Cama normal fault zones (Table 1). The maximum estimated geological throw of the Campo Felice fault is ~1050 m, with a possible overestimate of ~400 m (Fig. 2c). The fault scarp (3–15 m high) is continuous along-strike and composed of numerous segments arranged *én-echelon*. The fault core (40 cm–15 m thick) and highly fractured rocks domains (50–150 m thick and with fractures <3 cm spaced apart) are cut by numerous high-angle secondary faults and veins (Figs. 4 and 5). On the contrary, the Cama fault scarp (~2 m high) discontinuously outcrops only in the middle and southern sectors. The fault core is almost absent and fractures in the damage zone (<40 m thick) are usually spaced >10 cm apart, consistent with the ~100 m of maximum geological throw and the estimated low Quaternary throw rates estimated (Figs. 2d and 6). Furthermore, the numerous high-angle fissures affecting the footwall block and associated gravitative geomorphological structures (e.g., double-crested lines, scarps and counter-slope scarps) are coherent with an immature/incipient and small-displacement normal fault that is currently re-used by gravity to accommodate the lateral spreading of Mt. D'Ocre ridge. Therefore, the Cama fault is not expected to link at depth with the Campo Felice fault, whose damage zone shows architectural features consistent with what observed in other large-displacement normal fault zones in the central Apennines. According to this interpretation, the seismogenic source associated with the Ovindoli-L'Aquila Fault System would be reduced up to 8–9 km, thus reducing the maximum expected earthquake magnitude of the fault system from ~6.8 to ~6.5 (Wells and Coppersmith, 1994). However, the possible reduction of the seismogenic potential of the Ovindoli-L'Aquila Fault System is based on the hypothesis that the Cama fault is currently the shear zone of a lateral spreading DSGD and not linked at depth with the Campo Felice fault (Fig. 1d). Since in lateral spreading DGSDs the basal shear zone usually does not crop out (Varnes, 1978; Hutchinson, 1988; Agliardi et al., 2001, 2012; Dramis and smile-valvo, 1994; Discenza and Esposito, 2021) this hypothesis requires further geophysical investigations. Moreover, recent throw distribution and structural field analyses suggest a possible shallow soft-linkage to NW between the Campo Felice and Mt. Orsello faults, thus increasing the seismic potential of the fault system (Fig. 1; Schirripa Spagnolo et al., 2021).

The slip zone of the Campo Felice fault is a proto-cataclasite to cataclasite composed of angular to sub-rounded clasts (1–5 mm thick) surrounded by a fine matrix whose amount increases toward the slip surface (Fig. 8a). On the contrary, the slip zone of Cama fault is a mosaic breccia with 1–10 mm thick angular clasts cut by numerous fractures filled with sparite (Fig. 9a). The fine matrix of the Campo Felice fault slip zone is composed of calcite micro-grains with irregular to stylolitic-like boundaries and pores locally filled with oxides and clay minerals, with incipient triple junctions and indentation structures, interpreted as due to pressure-solution processes. Instead, the secondary sparite filling the fractures of the Cama fault slip zone is composed of blocky calcite grains, locally indented, with straight to irregular boundaries, due to rapid precipitation after fracturing at shallow crustal levels and pressure-solution processes (Fig. 9c and d). Such observations indicate how in carbonate-hosted normal faults, cataclasis and pressure-solution processes are the main deformation mechanisms active during sliding. These processes are much more active in the case of Campo Felice fault because of the larger displacement cumulated in time and amount of clay minerals with respect to the Cama fault, that allowed for a much higher grain comminution and lower grain boundary healing enhancing pressure-solution processes.

This work shows how the systematic study at macro-to micro-scale of fault zones can be integrated with geomorphological and geological analyses to provide further parameters to improve the characterization of seismogenic sources (Galadini et al., 2012; Falcucci et al., 2016).

Author statement

Luca Del Rio, Marco Moro, Michele Saroli, Giulio Di Toro: Conceptualization; Marco Moro, Giulio Di Toro: Funding acquisition; Luca Del Rio, Marco Moro, Simone Masoch, Andrea Cavallo, Fawzi Doumaz, Giulio Di Toro: Investigation; Giulio Di Toro, Marco Moro: Project Administration; Luca Del Rio, Marco Moro, Giulio Di Toro: Supervision; Luca Del Rio: Writing – original draft; Marco Moro, Giulio Di Toro, Michele Saroli, Simone Masoch: Writing – review & editing.

Declaration of competing interest

The authors declare that they have no known competing financial interests or personal relationships that could have appeared to influence the work reported in this paper.

Data availability

Data will be made available on request.

Acknowledgments

This research was funded by the European Research Council Consolidator Grant Project NOFEAR No 614705 (L.D.R., M.F. and G.D. T.), by the INGV projects: "*Caratterizzazione microstrutturale di piani di faglia attivi ed esumati e di piani di scivolamento di deformazioni gravitative profonde di versante (DGPV)*" and "Investigation of bedrock shear planes microstructures" and by a Marie Curie Fellowship (M.M.). S.M. acknowledges Fondazione CARIPARO for funding his PhD scholarship. We thank Leonardo Tauro for thin section preparation, Nicola Michelon for preparing field materials and thin section scans and Girolamo Dixit Dominus for support in field work. Fabrizio Agosta, Andrea Billi and an anonymous Reviewer are thanked for their constructive comments.

References

Agliardi, F., Crosta, G., Frattini, P., 2012. Slow rock-slope deformation. In: Clague, J.J., Stead, D. (Eds.), Landslides Types, Mechanisms and Modeling. Cambridge University Press, Cambridge, pp. 207–221.

Agliardi, F., Crosta, G., Zanchi, A., 2001. Structural constraints on deep-seated slope deformation kinematics. Eng. Geol. 59, 83–102. https://doi.org/10.1016/s0013-7952(00)00066-1.

Agosta, F., Aydin, A., 2006. Architecture and deformation mechanism of a basin bounding normal fault in Mesozoic platform carbonates, central Italy. J. Struct. Geol. 28 (8), 1445–1467. https://doi.org/10.1016/j.jsg.2006.04.006.

Aharonov, E., Katsman, R., 2009. Interaction between pressure solution and clays in stylolite development: insights from modeling. Am. J. Sci. 309 (7), 607–632.

Albano, M., Barba, S., Saroli, M., Moro, M., Malvarosa, F., Costantini, M., Bignami, C., Stramondo, S., 2015. Gravity-driven postseismic deformation following the Mw 6.3 2009 L'Aquila (Italy) earthquake. Sci. Rep. 5, 16558.

Allmendinger, R.W., Cardozo, N., Fisher, D., 2011. Structural Geology Algorithms: Vectors and Tensors. Cambridge University Press.

Andriani, G.F., Parise, M., 2015. On the applicability of geomechanical models for carbonate rock masses interested by karst processes. Environ. Earth Sci. 74, 7813–7821 (this special issue).

Billi, A., Salvini, F., Storti, F., 2003. The damage zone-fault core transition in carbonate rocks: implications for fault growth, structure and permeability. J. Struct. Geol. 25, 1779–1794.

Boncio, P., Lavecchia, G., Pace, B., 2004. Defining a model of 3D seismogenic sources for seismic hazard assessment applications: the case of central Apennines (Italy). J. Seismol. 8 (3), 407–425. https://doi.org/10.1023/b:jose.0000038449.78801.05.

Bons, P.D., Elburg, M.A., Gomez-Rivas, E., 2012. A review of the formation of tectonic veins and their microstructures. J. Struct. Geol. 43, 33–62. https://doi.org/10.1016/j.jsg.2012.07.005.

Bosi, C., Galadini, F., Messina, P., 1993. Neotectonic significance of bedrock fault scarps: case studies from the Lazio-Abruzzi Apennines (central Italy). Z. Geomorphol., Suppl.bd. 94, 187–206.

Bosi, C., Galadini, F., Giaccio, B., Messina, P., Sposato, A., 2003. Plio-Quaternary continental deposits in the Latium-Abruzzi Apennines: the correlation of geological events across different intermontane basins. Il Quat. 16, 55–76.

Bozzano, F., Bretschneider, A., Esposito, C., Martino, S., Prestininzi, A., Scarascia Mugnozza, G., 2013. - lateral spreading processes in mountain ranges: insights from an analogue modelling experiment. Tectonophysics 605, 88–95. https://doi.org/10.1016/j.tecto.2013.05.006.

Brandano, M., 2017. Unravelling the origin of a Paleogene unconformity in the Latium-Abruzzi carbonate succession: a shaved platform. Palaeogeogr. Palaeoclimatol. Palaeoecol. 485, 687–696.

Caine, J.S., Evans, J.P., Forster, C.B., 1996. Fault zone architecture and permeability structure. Geology 24 (11), 1025–1028. https://doi.org/10.1130/00917613(1996).

Caputo, R., Monaco, C., Tortorici, L., 2006. Multiseismic cycle deformation rates from Holocene normal fault scarps on Crete (Greece). Terra. Nova 18, 181–190.

Caputo, R., Catalano, S., Monaco, C., Romagnoli, G., Tortorici, G., Tortorici, L., 2010. Active faulting on the island of Crete (Greece). Geophys. J. Int. 183, 111–126.

Cardozo, N., Allmendinger, R.W., 2013. Spherical projections with OSX stereonet. Comput. Geosci. 51, 193–205. https://doi.org/10.1016/j.cageo.2012.07.021.

Carminati, E., Doglioni, C., 2012. Alps vs. Apennines: the paradigm of a tectonically asymmetric Earth. Earth Sci. Rev. 112 (1–2), 67–96. https://doi.org/10.1016/j.earscirev.2012.02.004.

Carminati, E., Lustrino, M., Doglioni, C., 2012. Geodynamic evolution of the central and western Mediterranean: tectonics vs. igneous petrology constraints. Tectonophysics 579, 173–192. https://doi.org/10.1016/j.tecto.2012.01.026.

Cavinato, G.P., Carusi, C., Dall'Asta, M., Miccadei, E., Piacentini, T., 2002. Sedimentary and tectonic evolution of Plio-Pleistocene alluvial and lacustrine deposits of the Fucino Basin (central Italy). Sediment. Geol. 148, 29–59. https://doi.org/10.1016/s0037-0738(01)00209-3.

Chester, F.M., Chester, J.S., 1998. Ultracataclasite structure and friction processes of the Punchbowl fault, San Andreas system, California. Tectonophysics 295, 199–221. https://doi.org/10.1016/s0040-1951(98)00121-8.

Chester, F.M., Logan, J.M., 1986. Implications for mechanical properties of brittle faults from observations of the Punchbowl fault zone, California. Pure Appl. Geophys. 124, 79–106.

Chester, F.M., Biegel, R.L., Evans, J.P., 1993. Internal structure and weakening mechanisms of the San-Andreas fault. J. Geophys. Res. Solid Earth 98, 771–786.

Chiaraluce, L., Di Stefano, R., Tinti, E., Scognamiglio, L., Michele, M., Casarotti, E., et al., 2017. The 2016 Central Italy seismic sequence: a first look at the mainshocks, aftershocks, and source models. Seismol Res. Lett. 88 (3), 757–771. https://doi.org/10.1785/0220160221.

Choi, J.H., Edwards, P., Ko, K., Kim, Y.S., 2016. Definition and classification of fault damage zones: a review and a new methodological approach. Earth Sci. Rev. 152, 70–87.

Clemenzi, L., Storti, F., Balsamo, F., Molli, G., Ellam, R., Muchez, P., Swenne, R., 2015. Fluid pressure cycles, variations in permeability, and weakening mechanisms along low-angle normal faults: the Tellaro detachment. Italy. Geol. Soc. Am. Bull. 127 (11–12), 1689–1710.

Cosentino, D., Cipollari, P., Marsili, P., Scrocca, D., 2010. Geology of the central apennines: a regional review. J. Virtual Explor. 36, 1–37.

Croizè, D., Renard, F., Gratier, J.P., 2013. Compaction and porosity reduction in carbonates: a review of observations, theory, and experiments. Adv. Geophys. 54, 181–238. https://doi.org/10.1016/b978-0-12-380940-7.00003-2.

Crosta, G.B., Frattini, P., Agliardi, F., 2013. Deep seated gravitational slope deformations in the European Alps. Tectonophysics 605, 13–33. https://doi.org/10.1016/j.tecto.2013.04.028.

D'Agostino, N., Giuliani, R., Mattone, M., Bonci, L., 2001. Active crustal extension in the central Apennines (Italy) inferred from GPS measurements in the interval 1994-1999. Geophys. Res. Lett. 28, 2121–2124. https://doi.org/10.1029/2000gl012462.

Damiani, A.V., Chiocchini, M., Colacicchi, R., Mariotti, G., Parotto, M., Passeri, L., Praturlon, A., 1992. Elementi litostratigrafici per una sintesi delle facies carbonatiche meso-cenozoiche dell'Appennino centrale. spec Studi Geol. Camerti 187–213, 1991/2.

Del Rio, L., Moro, M., Fondriest, M., Saroli, M., Gori, S., Falcucci, E., Cavallo, A., Doumaz, F., Di Toro, G., 2021. Active faulting and deep-seated gravitational slope deformation in carbonate rocks (central Apennines, Italy): a new "close-up" view. Tectonics 40. https://doi.org/10.1029/2021TC006698.

Demangeot, J., 1965. Géomorphologie des Abruzzes Adriatiques (Numero hors serie, vol. 403. Centre Recherche et Documentation Cartographiques Memoires et Documents.

Demurtas, M., Fondriest, M., Balsamo, F., Clemenzi, L., Storti, F., Bistacchi, A., Di Toro, G., 2016. Structure of a normal seismogenic fault zone in carbonates: the Vado di Corno fault, Campo Imperatore, central Apennines (Italy). J. Struct. Geol. 90, 185–206. https://doi.org/10.1016/j.jsg.2016.08.004.

Di maggio, C., Madonia, G., Vattano, M., 2014. deep-seated gravitational slope deformations in western sicily: controlling factors, triggering mechanisms, and morphoevolutionary models. Geomorphology 208, 173–189. https://doi.org/10.1016/j.geomorph.2013.11.023.

Di Toro, G., Pennacchioni, G., 2005. Fault plane processes and mesoscopic structure of a strong-type seismogenic fault in tonalites (Adamello batholith, Southern Alps). Tectonophysics 402 (1–4), 55–80. https://doi.org/10.1016/j.tecto.2004.12.036.

Discenza, M.E., Esposito, C., 2021. State-of-art and remarks on some open questions about DSGSDs: hints from a review of the scientific literature on related topics. Ital. J. Eng. Geol. Environ. 21 (1), 31–59.

Dramis, F., 1983. Morfogenesi di versante nel Pleistocene superiore in Italia: i depositi detritici stratificati. Geogr. Fis. Din. Quaternaria 6, 180–182.

Dramis, F., 1992. Il ruolo dei sollevamenti tettonici a lungo raggio nella genesi del rilievo appenninico. spec Studi Geol. Camerti 9–15, 1992/1.

Dramis, F., Sorriso-Valvo, M., 1994. Deep-seated gravitational slope deformations, related landslides and tectonics. Eng. Geol. 38, 231–243. https://doi.org/10.1016/0013-7952(94)90040-x.

Ehrenberg, S.N., McArthur, J.M., Thirlwall, M.F., 2006. Growth, demise, and dolomitization of miocene carbonate platforms on the Marion Plateau, o_shore NE Australia. J. Sediment. Res. 76 (1), 91–116.

Elter, P., Giglia, G., Tongiorgi, M., Trevisan, L., 1975. Tensional and compressional areas in the recent (Tortonian to present) evolution of the Northern Apennines. Boll. Geofis. Teor. Appl. 17, 3–18.

EMERGEO Working Group, 2010. Evidence for surface rupture associated with the MW 6.3 L'Aquila earthquake sequence of April 2009 (central Italy). Terra. Nova 22 (1), 43–51. https://doi.org/10.1111/j.1365-3121.2009.00915.x.

Engelder, T., 1987. Joints and shear fractures in rock. In: Atkinson, B.K. (Ed.), Fracture Mechanics of Rock. Academic Press, pp. 27–69. https://doi.org/10.1016/b978-0-12-066266-1.50007-7.

Falcucci, E., Gori, S., Galadini, F., Fubelli, G., Moro, M., Saroli, M., 2016. Active faults in the epicentral and mesoseismal Ml 6.0 24, 2016 Amatrice earthquake region, central Italy. Methodological and seismotectonic issues. Ann. Geophys. 59 https://doi.org/10.4401/ag-7266.

Faulkner, D.R., Lewis, A.C., Rutter, E.H., 2003. On the internal structure and mechanics of large strike-slip faults: field observations from the Carboneras fault, southeastern Spain. Tectonophysics 367, 235–251.

Faulkner, D.R., Jackson, C.A.L., Lunn, R.J., Schlische, R.W., Shipton, Z.K., Wibberley, C. A.J., Withjack, M.O., 2010. A review of recent developments concerning the structure, mechanics and fluid flow properties of fault zones. J. Struct. Geol. 32 (11), 1557–1575. https://doi.org/10.1016/j.jsg.2010.06.009.

Faulkner, D.R., Mitchell, T.M., Jensen, E., Cembrano, J., 2011. Scaling of fault damage zones with displacement and the implications for fault growth processes, 2011 J. Geophys. Res. 116. https://doi.org/10.1029/2010JB007788. Article B05403.

Ferraro, F., Grieco, D.S., Agosta, F., Prosser, G., 2018. Space-time evolution of cataclasis in carbonate fault zones. J. Struct. Geol. 110, 45–64.

Ferraro, F., Agosta, F., Ukar, E., Grieco, D.S., Cavalcante, F., Belviso, C., Prosser, G., 2019. Structural diagenesis of carbonate fault rocks exhumed from shallow crustal depths: an example from the central-southern Apennines, Italy. J. Struct. Geol. 122, 58–80.

Ferraro, F., Agosta, F., Prasad, M., Vinciguerra, S., Violay, M., Giorgioni, M., 2020. Pore space properties in carbonate fault rocks of peninsular Italy. J. Struct. Geol. 130, 103913.

Ferrarrini, F., De Nardis, R., Lavecchia, G., Brozzetti, F., 2015. Fault geometry and active stress from earthquakes and field geology data analysis: the Colfiorito 1997 and L'Aquila 2009 cases (Central Italy). Pure Appl. Geophys. 172 (5), 1079–1103. https://doi.org/10.1007/s00024-014-0931-7.

Fondriest, M., Balsamo, F., Bistacchi, A., Clemenzi, L., Demurtas, M., Storti, F., Di Toro, G., 2020. Structural complexity and mechanics of a shallow crustal seismogenic source (Vado di Corno Fault Zone, Italy). J. Geophys. Res. Solid Earth 125. https://doi.org/10.1029/2019JB018926.

Fossen, H., 2010. Structural Geology. Cambridge University Press, p. 463.

Galadini, F., 2006. Quaternary tectonics and large-scale gravitational deformations with evidence of rock-slide displacements in the Central Apennines (central Italy). Geomorphology 82, 201–228. https://doi.org/10.1016/j.geomorph.2006.05.003.

Galadini, F., Galli, P., 2000. Active tectonics in the central Apennines (Italy)—input data for seismic hazard assessment. Nat. Hazards 22, 225–268. https://doi.org/10.1023/a:1008149531980.
Galadini, F., Galli, P., 2003. Paleoseismology of silent faults in the central apennines (Italy): the Mt. Vettore and laga Mts. Faults. Ann. Geophis. 46, 815–836.
Galadini, F., Falcucci, E., Galli, P., Giaccio, B., Gori, S., Messina, P., Moro, M., Saroli, M., Scardia, G., Sposato, A., 2012. Time intervals to assess active and capable faults for engineering practices in Italy. Eng. Geol. 139–140, 50–65.
Galli, P., Galadini, F., Pantosti, D., 2008. Twenty years of paleoseismology in Italy. Earth Sci. Rev. 88, 89–117. https://doi.org/10.1016/j.earscirev.2008.01.001.
Giraudi, C., Bodrato, G., Lucchi, M.R., Cipriani, N., Villa, I.M., Giaccio, B., Zuppi, G.M., 2011. Middle and late Pleistocene glaciations in the Campo Felice basin (central apennines, Italy). Quat. Res. 75 (1), 219–230. https://doi.org/10.1016/j.yqres.2010.06.006.
Gomila, R., Arancibia, G., Mitchell, T.M., Cembrano, J.M., Faulkner, D.R., 2016. Palaeopermeability structure within fault-damage zones: a snap-shot from microfracture analyses in a strike-slip system. J. Struct. Geol. 83, 103–120. https://doi.org/10.1016/j.jsg.2015.12.002.
Gratier, J.P., Dysthe, D., Renard, F., 2013. The role of pressure solution creep in the ductility of the Earth's upper crust. Adv. Geophys. 54, 47–179. https://doi.org/10.1016/b978-0-12-380940-7.00002-0.
Gundersen, E., Renard, F., Dysthe, D.K., Bjorlykke, K., Jamtveit, B., 2002. Coupling between pressure solution creep and diffusive mass transport in porous rocks. J. Geophys. Res. Solid Earth 107. https://doi.org/10.1029/2001JB000287.
Hunstad, I., Selvaggi, G., D'Agostino, N., England Clarke, P., Pierozzi, M., 2003. Geodetic strains in peninsular Italy between 1875 and 2001. Geophys. Res. Lett. 30, 1828.
Hutchinson, J.N., 1988. General report: morphological and geotechnical parameters of landslides in relation to geology and hydrogeology. Lausanne, CH. In: Proceedings of the 5th International Symposium on Landslides, vol. 1. Balkema, Rotterdam, 3±35.
Jaboyedoff, M., Penna, I., Pedrazzini, A., Baroň, I., Crosta, G.B., 2013. An introductory review on gravitational-deformation induced structures, fabrics and modeling. Tectonophysics 605, 1–12. https://doi.org/10.1016/j.tecto.2013.06.027.
Jahn, A., 1964. Slow morphological features resulting from gravitation. Z. Geomorphol. 5, 59–72.
Kim, Y.S., Peacock, D.C.P., Sanderson, D.J., 2004. Fault damage zones. J. Struct. Geol. 26 (3), 503–517.
La Bruna, V., Agosta, F., Lamarche, J., Viseur, S., Prosser, G., 2018. Fault growth mechanisms and scaling properties in foreland basin system: the case study of Monte Alpi, Southern Apennines, Italy. J. Struct. Geol. 116, 94–113.
Lavecchia, G., Brozzetti, F., Barchi, M., Menichetti, M., Keller, J.V.A., 1994. Seismotectonic zoning in east-central Italy deduced from an analysis of the Neogene to present deformations and related stress fields. Geol. Soc. Am. Bull. 106 (9), 1107–1120. https://doi.org/10.1130/0016-7606(1994)106<1107:SZIECI>2.3.CO;2.
Leah, H., Fondriest, M., Lucca, A., Storti, F., Balsamo, F., Di Toro, G., 2018. Coseismic extension recorded within the damage zone of the vado di Ferruccio thrust fault, central apennines, Italy. J. Struct. Geol. 114, 121–138. https://doi.org/10.1016/j.jsg.2018.06.015.
Lehner, F.K., 1995. A model for intergranular pressure solution in open systems. Tectonophysics 245, 153–170.
Leonard, M., 2010. Earthquake fault scaling: self-consistent relating of rupture length, width, average displacement, and moment release. Bull. Seismol. Soc. Am. 100 (5A), 1971–1988.
Lucca, A., Storti, F., Balsamo, F., Clemenzi, L., Fondriest, M., Burgess, R., Di Toro, G., 2019. From submarine to subaerial out-of-sequence thrusting and gravity-driven extensional faulting: gran Sasso massif, central Apennines, Italy. Tectonics 38, 4155–4184. https://doi.org/10.1029/2019tc005783.
Malinverno, A., Ryan, W.B.F., 1986. Extension in the Tyrrhenian Sea and shortening in the Apennines as result of arc migration driven by sinking of the lithosphere. Tectonics 5, 227–245. https://doi.org/10.1029/tc005i002p00227.
Mancinelli, A., Chiocchini, M., Coccia, B., 2003. Orbitolinidae and Alveolinidae (Foraminiferida) from the uppermost Albian-lower Cenomanian of Monti d'Ocre (Abruzzi, Italy). Cretac. Res. 24, 729–741.
Mancinelli, P., Scisciani, V., Patruno, S., Minelli, G., 2021. Gravity modeling reveals a Messinian foredeep depocenter beneath the intermontane Fucino basin (central Apennines). Tectonophysics 821, 229144. https://doi.org/10.1016/j.tecto.2021.229144.
Marshak, S., Haq, S.S.B., Sen, P., 2019. Ramp initiation in fold-thrust belts: insight from PIV analysis of sandbox models. J. Struct. Geol. 118, 308–323.
Masoch, S., Fondriest, M., Preto, N., Secco, M., Di Toro, G., 2019. Seismic cycle recorded in cockade-bearing faults (Col de Teghime, Alpine Corsica). J. Struct. Geol. 129, 103889 https://doi.org/10.1016/j.jsg.2019.103889.
Masoch, S., Gomila, R., Fondriest, M., Jensen, E., Mitchell, T., Pennacchioni, G., Cembrano, J., Di Toro, G., 2021. Structural evolution of a crustal-scale seismogenic fault in a magmatic arc: the bolfin fault zone (Atacama Fault System). Tectonics 40. https://doi.org/10.1029/2021TC006818.
Masoch, S., Fondriest, M., Gomila, R., Jensen, E., Mitchell, T., Cembrano, J., Pennacchioni, G., Di Toro, G., 2022. Along-strike architectural variability of an exhumed crustal-scale seismogenic fault (Bolfin Fault Zone, Atacama Fault System, Chile). J. Struct. Geol. 165, 104745.
Mayolle, S., Soliva, R., Caniven, Y., Wibberley, C., Ballas, G., Milesi, G., Dominguez, S., 2019. Scaling of fault damage zones in carbonate rocks. J. Struct. Geol. 124, 35–50.
Mitchell, T.M., Faulkner, D.R., 2009. The nature and origin of off fault damage surrounding strike-slip fault zones with a wide range of displacements: a field study from the Atacama fault system, northern Chile. J. Struct. Geol. 31, 802–816. https://doi.org/10.1016/j.jsg.2009.05.002.
Ostermeijer, G., Mitchell, T., Aben, F., Dorsey, M., Rockwell, T., Fletcher, J., Ostermeijer, F., 2020. Damage zone heterogeneity on seismogenic faults in crystalline rock; a field study of the Borrego Fault, Baja California. J. Struct. Geol. 137, 104016 https://doi.org/10.1016/j.jsg.2020.104016.
Panek, T., Klimeš, J., 2016. Temporal behavior of deep-seated gravitational slope deformations: a review. Earth Sci. Rev. 156, 14–38.
Pantosti, D., D'Addezio, G., Cinti, F.R., 1996. Paleoseismicity of the Ovindoli– Pezza fault, Central Apennines, Italy: a history including a large previously unrecorded earthquake in middle Ages (890-1300). J. Geophys. Res. 101, 5937–5959.
Patacca, E., Scandone, P., 1989. Post-Tortonian mountain building in the Apennines. The role of the passive sinking of a relic lithospheric slab. In: Boriani, A., Bonafede, M., Piccardo, G.B., Atti dei Convegni Lincei, Vai G.B. (Eds.), The Lithosphere in Italy, vol. 80, pp. 157–176.
Patacca, E., Sartori, R., Scandone, P., 1992. Tyrrhenian basin and Apenninic arcs: kinematic relations since late Tortonian times. Mem. Soc. Geol. It. 45, 425–451.
Petit, J.P., 1987. Criteria for the sense of movement on fault surfaces in brittle rocks. J. Struct. Geol. 9 (5-6), 597–608. https://doi.org/10.1016/0191-8141(87)90145-3.
Pollard, D., Aydin, A., 1988. Progress in understanding jointing over the past century. Geol. Soc. Am. Bull. 100, 1181–1204. https://doi.org/10.1130/0016-7606(1988)100<1181:piujot>2.3.co;2.
Power, W.L., Tullis, T.E., 1989. The relationship between slickenside surfaces in fine-grained quartz and the seismic cycle. J. Struct. Geol. 11, 879–894.
Renard, F., Gratier, J.P., Jamtveit, B., 2000. Kinetics of crack-sealing, intergranular pressure solution, and compaction around active faults. J. Struct. Geol. 22 (10), 1395–1407. https://doi.org/10.1016/s0191-8141(00)00064-x.
Renard, F., Dysthe, D., Feder, J., Bjørlykke, K., Jamtveit, B., 2001. Enhanced pressure solution creep rates induced by clay particles: experimental evidence in salt aggregates. Geophys. Res. Lett. 28, 1295–1298. https://doi.org/10.1029/2000gl012394.
Rotevatn, A., Bastesen, E., 2012. Fault linkage and damage zone architecture in tight carbonate rocks in the Suez Rift (Egypt): implications for permeability structure along segmented normal faults. Geol. Soc. Lond. Spec. Publ. 374 https://doi.org/10.1144/SP374.12.
Rovida, A., Locati, M., Camassi, R., Lolli, B., Gasperini, P., 2020. The Italian earthquake catalogue CPTI15. Bull. Earthq. Eng. 18, 2953–2984. https://doi.org/10.1007/s10518-020-00818-y.
Rowe, C.D., Griffith, W.A., 2015. Do faults preserve a record of seismic slip: a second opinion. J. Struct. Geol. 78, 1–26.
Rutter, E.H., 1983. Pressure solution in nature, theory and experiment. J. Geol. Soc. 140, 725–740. https://doi.org/10.1144/gsjgs.140.5.0725.
Salvi, S., Nardi, A., 1995. The Ovindoli Fault: a segment of a longer, active fault zone in central Abruzzi, Italy. In: Serva, L., Slemmons, D.B. (Eds.), In Perspectives in Paleoseismology, vol. 6, pp. 101–113 (Bull. Assoc. Eng. Geol).
Salvi, S., Cinti, F.R., Colini, L., D'addezio, G., Doumaz, F., Pettinelli, E., 2003. Investigation of the active Celano-L'Aquila fault system, Abruzzi (central Apennines, Italy) with combined ground-penetrating radar and paleoseismic trenching. Geophys. J. Int. 155 (3), 805–818. https://doi.org/10.1111/j.1365-246X.2003.02078.x.
Savage, H.M., Brodsky, E.E., 2011. Collateral damage: evolution with displacement of fracture distribution and secondary fault strands in fault damage zones. J. Geophys. Res. 116, B03405 https://doi.org/10.1029/2010JB007665.
Schirripa Spagnolo, G., Mercuri, M., Billi, A., Carminati, E., Galli, P., 2021. The segmented Campo Felice normal faults: seismic potential appraisal by application of empirical relationships between rupture length and earthquake magnitude in the central Apennines. Italy Tectonics 40 (7).
Sibson, R.H., 1977. Fault rocks and fault mechanisms. Geol. Soc. London J. 133, 191–213. https://doi.org/10.1144/gsjgs.133.3.0191.
Sibson, R.H., 1986. Earthquakes and rock deformation in crustal fault zones. Annu. Rev. Earth Planet Sci. 14, 149–175.
Sibson, R.H., 2003. Thickness of the seismic slip zone. Bull. Seismol. Soc. Am. 93, 1169–1178. https://doi.org/10.1785/0120020061.
Smith, S.A.F., Billi, A., Di Toro, G., Spiess, R., 2011. Principal slip zones in limestone: microstructural characterization and implications for the seismic cycle (Tre Monti fault, Central Apennines, Italy). Pure Appl. Geophys. 168 (12), 2365–2393. https://doi.org/10.1007/s00024-011-0267-5.
Smith, S.A.F., Nielsen, S., Di Toro, G., 2015. Strain localization and the onset of dynamic weakening in calcite fault gouge. Earth Planet Sci. Lett. 413, 25–36.
Tada, R., Siever, R., 1989. Pressure solution during diagenesis. Annu. Rev. Earth Planet Sci. 17, 89–118. https://doi.org/10.1146/annurev.ea.17.050189.000513.
Tarquini, S., Isola, I., Favalli, M., Mazzarini, F., Bisson, M., Pareschi, M.T., Boschi, E., 2007. TINITALY/01: a new triangular irregular network of Italy. Ann. Geophys. 50, 407–425.
Tesei, T., Collettini, C., Viti, C., Barchi, M.R., 2013. Fault architecture and deformation mechanisms in exhumed analogues of seismogenic carbonate-bearing thrusts. J. Struct. Geol. 55, 167–181.
Varnes, D.J., 1978. Slope movements types and processes. In: Schuster, R.L., Krizek, R.J. (Eds.), Landslides: Analysis and Control, pp. 11–35.
Verhaert, G., Muchez, P., Keppens E, E., Sintubin, M., 2009. Fluid impact and spatial and temporal evolution of normal faulting in limestones. A case study in the Burdur-Isparta Region (SW Turkey). Geol. Belg. 12, 59–73.
Vezzani, L., Festa, A., Ghisetti, F.C., 2010. Geology and Tectonic Evolution of the Central-Southern Apennines, Italy, vol. 469. Geological Society of America Special Paper, pp. 1–58. https://doi.org/10.1130/2010.2469.
Villani, F., Pucci, S., Civico, R., De Martini, P.M., Cinti, F.R., Pantosti, D., 2018. Surface faulting of the 30 October 2016 Mw 6.5 Central Italy earthquake: detailed analysis of

a complex coseismic rupture. Tectonics 37, 3378–3410. https://doi.org/10.1029/2018TC005175.
Wells, D.L., Coppersmith, K.J., 1994. New empirical relationships among magnitude, rupture length, rupture width, rupture area, and surface displacement. Bull. Seismol. Soc. Am. 84 (4), 974–1002.
Wesnousky, S.G., 2008. Displacement and geometrical characteristics of earthquake surface ruptures: Issues and implications for seismic-hazard analysis and the process of earthquake rupture. Bull. Seismol. Soc. Am. 98 (4), 1609–1632.
Wibberley, C.A.J., Yielding, G., Di Toro, G., 2008. Recent advances in the understanding of fault zone internal structure: a review. Geol. Soc. Lond. Spec. Publ. 299, 5–33. https://doi.org/10.1144/SP299.2.
Wilkinson, M., Roberts, G.P., McCaffrey, K., Cowie, P.A., Walker, J.P.F., Papanikolaou, I., Richard, J.P., Michetti, A.M., Vittori, E., Gregory, L., Wedmore, L., Watson, Z.K., 2015. Slip distributions on active normal faults measured from LiDAR and field mapping of geomorphic offsets: an example from L'Aquila, Italy, and implications for modelling seismic moment release. Geomorphology 237, 130–141.
Woodcock, N.H., Mort., K., 2008. Classification of fault breccias and related fault rocks. Geol. Mag. 145 (3), 435–440.